cent listing of titles in the *Artech House Universal Personal Communications Library*, turn to the back of this book.

OFDM Wireless Multimedia Communications

Richard van Nee
Ramjee Prasad

Artech House
Boston • London

Library of Congress Cataloging-in-Publication Data
Nee, Richard van.
OFDM for wireless multimedia communications / Richard van Nee, Ramjee Prasad
p. cm. — (Artech House universal personal communications library)
Includes bibliographical references and index.
ISBN 0-89006-530-6 (alk. paper)
1. Wireless communications systems. 2. Multimedia systems. 3. Multiplexing. I. Prasad, Ramjee. II. Title III. Series

TK5103.2.N44 2000 99-052312
621/3845—dc21 CIP

British Library Cataloguing in Publication Data
Nee, Richard van
OFDM wireless multimedia communications. — (Artech House universal personal communications library)
1.Wireless communications systems 2. Multimedia systems
I. Title II. Prasad, Ramjee
621.3'82

ISBN 0-89006-530-6

Cover design by Igor Vladman

International Standard Book Number: 0-89006-530-6
Library of Congress Catalog Card Number: 99-052312

10 9 8 7 6 5 4 3 2 1

Richard van Nee, Ramjee Prasad
munications library)

ia systems. 3. Multiplexing. I.

99-052312
CIP

Artech House

systems

2

To my wife Iris, to our son Floris, to our daughters Roselinde and Mirrelijn, and to our newly born baby
—Richard van Nee

To my wife Jyoti, to our daughter Neeli, and to our sons Anand and Rajeev
—Ramjee Prasad

Contents

Chapter 2

OFDM Basics

2.1 INTRODUCTION

The basic principle of OFDM is to split a high-rate datastream into a number of lower rate streams that are transmitted simultaneously over a number of subcarriers. Because the symbol duration increases for the lower rate parallel subcarriers, the relative amount of dispersion in time caused by multipath delay spread is decreased. Intersymbol interference is eliminated almost completely by introducing a guard time in every OFDM symbol. In the guard time, the OFDM symbol is cyclically extended to avoid intercarrier interference. This whole process of generating an OFDM signal and the reasoning behind it are described in detail in sections 2.2 to 2.4.

In OFDM system design, a number of parameters are up for consideration, such as the number of subcarriers, guard time, symbol duration, subcarrier spacing, modulation type per subcarrier, and the type of forward error correction coding. The choice of parameters is influenced by system requirements such as available bandwidth, required bit rate, tolerable delay spread, and Doppler values. Some requirements are conflicting. For instance, to get a good delay spread tolerance, a large number of subcarriers with a small subcarrier spacing is desirable, but the opposite is true for a good tolerance against Doppler spread and phase noise. These design issues are discussed in Section 2.5. Section 2.6 gives an overview of OFDM signal processing functions, while Section 2. ends this chapter with a complexity comparison of OFDM versus single-carrier systems.

2.2 GENERATION OF SUBCARRIERS USING THE IFFT

An OFDM signal consists of a sum of subcarriers that are modulated by using *phase shift keying (PSK)* or *quadrature amplitude modulation (QAM)*. If d_i are the complex

QAM symbols, N_s is the number of subcarriers, T the symbol duration, and f_c the carrier frequency, then one OFDM symbol starting at $t = t_s$ can be written as

$$s(t) = \mathrm{Re}\left\{ \sum_{i=-\frac{N_s}{2}}^{\frac{N_s}{2}-1} d_{i+N_s/2} \exp\left(j2\pi\left(f_c - \frac{i+0.5}{T}\right)(t-t_s)\right) \right\} \quad , t_s \le t \le t_s + T \tag{2.1}$$

$$s(t) = 0 \,, \quad t < t_s \ \wedge \ t > t_s + T$$

In the literature, often the equivalent complex baseband notation is used, which is given by (2.2). In this representation, the real and imaginary parts correspond to the in-phase and quadrature parts of the OFDM signal, which have to be multiplied by a cosine and sine of the desired carrier frequency to produce the final OFDM signal. Figure 2.1 shows the operation of the OFDM modulator in a block diagram.

$$s(t) = \sum_{i=-\frac{N_s}{2}}^{\frac{N_s}{2}-1} d_{i+N_s/2} \exp\left(j2\pi \frac{i}{T}(t-t_s)\right) \quad , t_s \le t \le t_s + T \tag{2.2}$$

$$s(t) = 0 \,, \quad t < t_s \ \wedge \ t > t_s + T$$

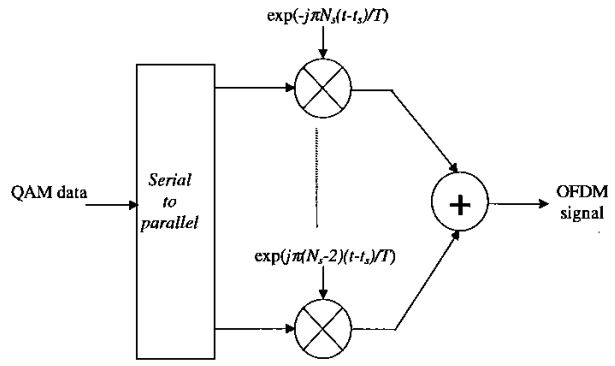

Figure 2.1 OFDM modulator.

As an example, Figure 2.2 shows four subcarriers from one OFDM signal. In this example, all subcarriers have the same phase and amplitude, but in practice the amplitudes and phases may be modulated differently for each subcarrier. Note that each subcarrier has exactly an integer number of cycles in the interval T, and the number of cycles between adjacent subcarriers differs by exactly one. This property accounts for

symbol duration, and f_c the carrier
an be written as

$$-t_s))\Big\}\ ,\ t_s \le t \le t_s + T \qquad (2.1)$$

baseband notation is used, which
imaginary parts correspond to the
which have to be multiplied by a
produce the final OFDM signal.
tor in a block diagram.

$$t_s \le t \le t_s + T \qquad (2.2)$$

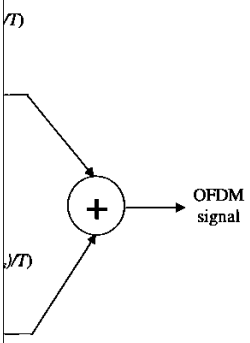

ator.

arriers from one OFDM signal. In
and amplitude, but in practice the
for each subcarrier. Note that each
n the interval T, and the number of
ly one. This property accounts for

the orthogonality between the subcarriers. For instance, if the jth subcarrier from (2.2) is demodulated by downconverting the signal with a frequency of j/T and then integrating the signal over T seconds, the result is as written in (2.3). By looking at the intermediate result, it can be seen that a complex carrier is integrated over T seconds. For the demodulated subcarrier j, this integration gives the desired output $d_{j+N/2}$ (multiplied by a constant factor T), which is the QAM value for that particular subcarrier. For all other subcarriers, the integration is zero, because the frequency difference $(i-j)/T$ produces an integer number of cycles within the integration interval T, such that the integration result is always zero.

$$\int_{t_s}^{t_s+T} \exp(-j2\pi\frac{j}{T}(t-t_s)) \sum_{i=-\frac{N_s}{2}}^{\frac{N_s}{2}-1} d_{i+N_s/2} \exp(j2\pi\frac{i}{T}(t-t_s))\,\mathrm{d}t$$
$$= \sum_{i=-\frac{N_s}{2}}^{\frac{N_s}{2}-1} d_{i+N_s/2} \int_{t_s}^{t_s+T} \exp(j2\pi\frac{i-j}{T}(t-t_s))dt = d_{j+N_s/2}T \qquad (2.3)$$

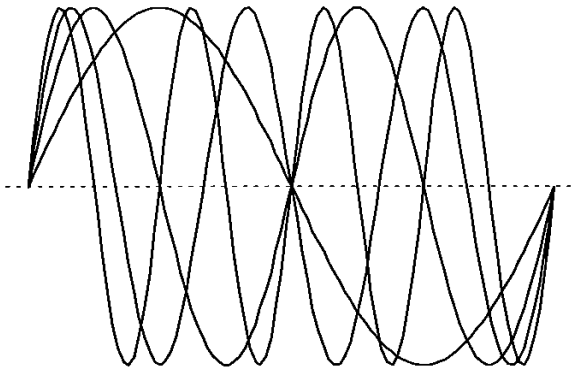

Figure 2.2 Example of four subcarriers within one OFDM symbol.

The orthogonality of the different OFDM subcarriers can also be demonstrated in another way. According to (2.1), each OFDM symbol contains subcarriers that are nonzero over a T-second interval. Hence, the spectrum of a single symbol is a convolution of a group of Dirac pulses located at the subcarrier frequencies with the spectrum of a square pulse that is one for a T-second period and zero otherwise. The amplitude spectrum of the square pulse is equal to $\mathrm{sinc}(\pi fT)$, which has zeros for all frequencies f that are an integer multiple of $1/T$. This effect is shown in Figure 2.2, which shows the overlapping sinc spectra of individual subcarriers. At the maximum of each subcarrier spectrum, all other subcarrier spectra are zero. Because an OFDM

receiver essentially calculates the spectrum values at those points that correspond to the maxima of individual subcarriers, it can demodulate each subcarrier free from any interference from the other subcarriers. Basically, Figure 2.3 shows that the OFDM spectrum fulfills Nyquist's criterium for an intersymbol interference free pulse shape. Notice that the pulse shape is present in the frequency domain and not in the time domain, for which the Nyquist criterium usually is applied. Therefore, instead of intersymbol interference (ISI), it is intercarrier interference (ICI) that is avoided by having the maximum of one subcarrier spectrum correspond to zero crossings of all the others.

The complex baseband OFDM signal as defined by (2.2) is in fact nothing more than the inverse Fourier transform of N_s QAM input symbols. The time discrete equivalent is the inverse discrete Fourier transform (IDFT), which is given by (2.4), where the time t is replaced by a sample number n. In practice, this transform can be implemented very efficiently by the inverse fast Fourier transform (IFFT). An N point IDFT requires a total of N^2 complex multiplications—which are actually only phase rotations. Of course, there are also additions necessary to do an IDFT, but since the hardware complexity of an adder is significantly lower than that of a multiplier or phase rotator, only the multiplications are used here for comparison. The IFFT drastically reduces the amount of calculations by exploiting the regularity of the operations in the IDFT. Using the radix-2 algorithm, an N-point IFFT requires only $(N/2)\cdot\log_2(N)$ complex multiplications [1]. For a 16-point transform, for instance, the difference is 256 multiplications for the IDFT versus 32 for the IFFT—a reduction by a factor of 8! This difference grows for larger numbers of subcarriers, as the IDFT complexity grows quadratically with N, while the IFFT complexity only grows slightly faster than linear.

$$s(n) = \sum_{i=0}^{N_s-1} d_i \exp(j2\pi \frac{in}{N}) \tag{2.4}$$

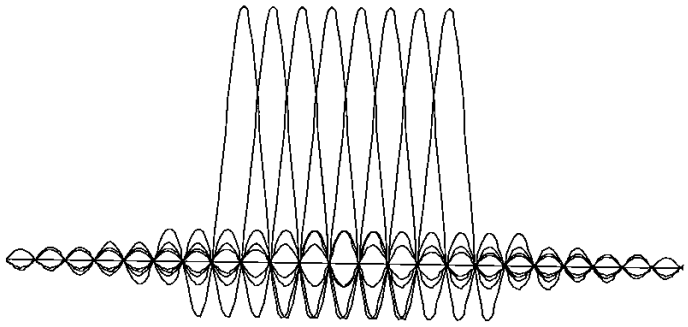

Figure 2.3 Spectra of individual subcarriers.

those points that correspond to the
te each subcarrier free from any
Figure 2.3 shows that the OFDM
ıbol interference free pulse shape.
ency domain and not in the time
pplied. Therefore, instead of inter-
ce (ICI) that is avoided by having
to zero crossings of all the others.

ıed by (2.2) is in fact nothing more
nput symbols. The time discrete
(IDFT), which is given by (2.4),
In practice, this transform can be
ırier transform (IFFT). An N point
ıs—which are actually only phase
sary to do an IDFT, but since the
er than that of a multiplier or phase
comparison. The IFFT drastically
regularity of the operations in the
IFFT requires only $(N/2)\cdot\log_2(N)$
rm, for instance, the difference is
FFT—a reduction by a factor of 8!
ers, as the IDFT complexity grows
grows slightly faster than linear.

$$\frac{n}{\sqrt{}}) \qquad (2.4)$$

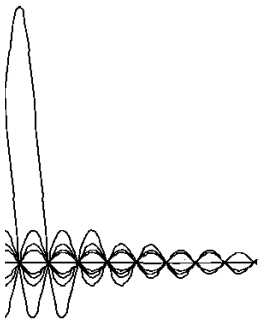

subcarriers.

The number of multiplications in the IFFT can be reduced even further by using a radix-4 algorithm. This technique makes use of the fact that in a four-point IFFT, there are only multiplications by $\{1,-1,j,-j\}$, which actually do not need to be implemented by a full multiplier, but rather by a simple add or subtract and a switch of real and imaginary parts in the case of multiplications by j or $-j$. In the radix-4 algorithm, the transform is split into a number of these trivial four-point transforms, and non-trivial multiplications only have to be performed between stages of these four-point transforms. In this way, an N-point FFT uslng the radix-4 algorithm requires only $(3/8)N(\log_2 N-2)$ complex multiplications or phase rotations and $N\log_2 N$ complex additions [1]. For a 64-point FFT, for example, this means 96 rotations and 384 additions, or 1.5 and 6 rotations and additions per sample, respectively.

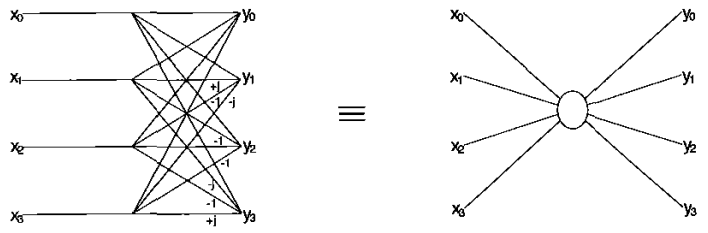

Figure 2.4 The radix-4 butterfly.

Figure 2.4 shows the four-point IFFT, which is known as the *radix-4 butterfly* that forms the basis for constructing larger IFFT sizes [1]. Four input values x_0 to x_3 are transformed into output values y_0 to y_3 by simple additions and trivial phase rotations. For instance, y_1 is given by $x_0 + jx_1 - x_2 - jx_3$, which can be calculated by doing four additions plus a few additional I/Q swappings and inversions to account for the multiplications by j and -1.

The radix-4 butterfly can be used to efficiently build an IFFT with a larger size. For instance, a 16-point IFFT is depicted in Figure 2.5. The 16-point IFFT contains two stages with four radix-4 butterflies, separated by an intermediate stage where the 16 intermediate results are phase rotated by the twiddle factor ω^i, which is defined as $exp(j2\pi i/N)$. Notice that for N=16, rotation by the twiddle factor ω^i reduces to a trivial operation for i=0, 4, 8 and 12, where ω^i is 1, j, –1 and $-j$, respectively. Taking this into account, the 16-point IFFT actually contains only eight non-trivial phase rotations, which is a factor of 32 smaller than the amount of phase rotations for the IDFT. These non-trivial phase rotations largely determine the implementation complexity, because the complexity of a phase rotation or complex multiplication is an order of magnitude larger than the complexity of an addition.

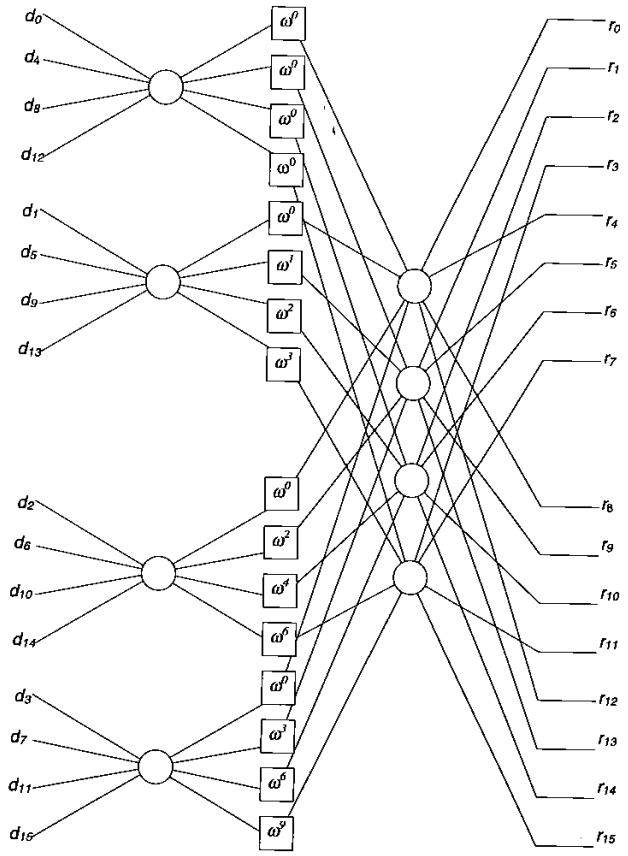

Figure 2.5 16-point IFFT using the radix-4 algorithm.

As an example of how to generate an OFDM symbol, let us assume that we want to transmit eight binary values {1 1 1 –1 1 1 –1 1} on eight subcarriers. The IDFT or IFFT then has to calculate:

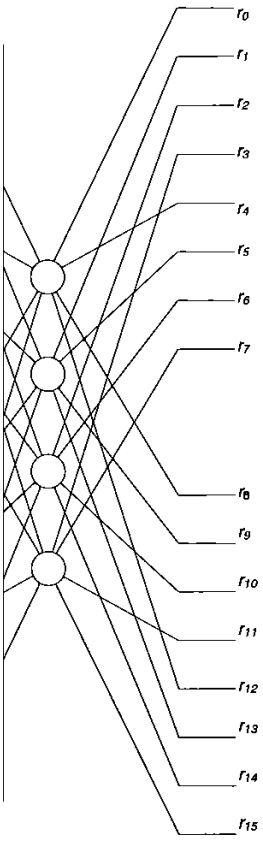

adix-4 algorithm.

)M symbol, let us assume that we
1} on eight subcarriers. The IDFT

$$\frac{1}{8}\begin{bmatrix} 1 & 1 & 1 & 1 & 1 & 1 & 1 & 1 \\ 1 & \frac{1}{2}\sqrt{2}(1+j) & j & \frac{1}{2}\sqrt{2}(-1+j) & -1 & \frac{1}{2}\sqrt{2}(-1-j) & -j & \frac{1}{2}\sqrt{2}(1-j) \\ 1 & j & -1 & -j & 1 & j & -1 & -j \\ 1 & \frac{1}{2}\sqrt{2}(-1+j) & -j & \frac{1}{2}\sqrt{2}(1+j) & -1 & \frac{1}{2}\sqrt{2}(1-j) & j & \frac{1}{2}\sqrt{2}(-1-j) \\ 1 & -1 & 1 & -1 & 1 & -1 & 1 & -1 \\ 1 & \frac{1}{2}\sqrt{2}(-1-j) & j & \frac{1}{2}\sqrt{2}(1-j) & -1 & \frac{1}{2}\sqrt{2}(1+j) & -j & \frac{1}{2}\sqrt{2}(-1+j) \\ 1 & -j & -1 & j & 1 & -j & -1 & j \\ 1 & \frac{1}{2}\sqrt{2}(1-j) & -j & \frac{1}{2}\sqrt{2}(-1-j) & -1 & \frac{1}{2}\sqrt{2}(-1+j) & j & \frac{1}{2}\sqrt{2}(1+j) \end{bmatrix} \begin{bmatrix} 1 \\ 1 \\ 1 \\ -1 \\ 1 \\ 1 \\ -1 \\ 1 \end{bmatrix} = \frac{1}{8}\begin{bmatrix} 4 \\ \sqrt{2}(1+j(\sqrt{2}-1)) \\ 2+2j \\ -\sqrt{2}(1+j(\sqrt{2}+1)) \\ 0 \\ -\sqrt{2}(1-j(\sqrt{2}+1)) \\ 2-2j \\ \sqrt{2}(1-j(\sqrt{2}-1)) \end{bmatrix} \tag{2.5}$$

The left-hand side of (2.5) contains the IDFT matrix, where every column corresponds to a complex subcarrier with a normalized frequency ranging from -4 to +3. The right-hand side of (2.5) gives the eight IFFT output samples that form one OFDM symbol. In practice, however, these samples are not enough to make a real OFDM signal. The reason is that there is no oversampling present, which would introduce intolerable aliasing if one would pass these samples though a digital-to-analog converter. To introduce oversampling, a number of zeros can be added to the input data. For instance, eight zeros could be added to the eight input samples of the previous example, after which a 16-point IFFT can be performed to get 16 output samples of a twice-oversampled OFDM signal. Notice that in the complex IFFT as in (2.5), the first half of the rows correspond to positive frequencies while the last half correspond to negative frequencies. Hence, if oversampling is used, the zeros should be added in the middle of the data vector rather than appending them at the end. This ensures the zero data values are mapped onto frequencies close to plus and minus half the sampling rate, while the nonzero data values are mapped onto the subcarriers around 0 Hz. For the data of the previous example, the oversampled input vector would become {1 1 1 –1 0 0 0 0 0 0 0 0 1 1 –1 1}.

2.3 GUARD TIME AND CYCLIC EXTENSION

One of the most important reasons to do OFDM is the efficient way it deals with multipath delay spread. By dividing the input datastream in N_s subcarriers, the symbol duration is made N_s times smaller, which also reduces the relative multipath delay spread, relative to the symbol time, by the same factor. To eliminate intersymbol interference almost completely, a guard time is introduced for each OFDM symbol. The guard time is chosen larger than the expected delay spread, such that multipath components from one symbol cannot interfere with the next symbol. The guard time could consist of no signal at all. In that case, however, the problem of intercarrier interference (ICI) would arise. ICI is crosstalk between different subcarriers, which means they are no longer orthogonal. This effect is illustrated in Figure 2.6. In this example, a subcarrier 1 and a delayed subcarrier 2 are shown. When an OFDM receiver

tries to demodulate the first subcarrier, it will encounter some interference from the second subcarrier, because within the FFT interval, there is no integer number of cycles difference between subcarrier 1 and 2. At the same time, there will be crosstalk from the first to the second subcarrier for the same reason.

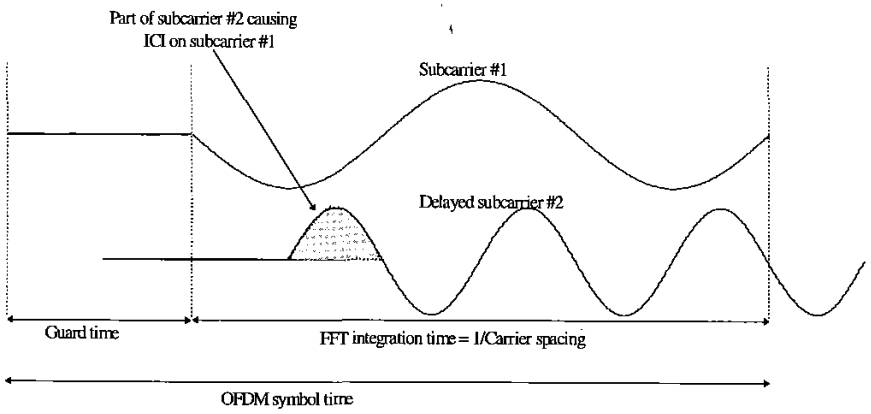

Figure 2.6 Effect of multipath with zero signal in the guard time; the delayed subcarrier 2 causes ICI on subcarrier 1 and vice versa.

To eliminate ICI, the OFDM symbol is cyclically extended in the guard time, as shown in Figure 2.7. This ensures that delayed replicas of the OFDM symbol always have an integer number of cycles within the FFT interval, as long as the delay is smaller than the guard time. As a result, multipath signals with delays smaller than the guard time cannot cause ICI.

As an example of how multipath affects OFDM, Figure 2.8 shows received signals for a two-ray channel, where the dotted curve is a delayed replica of the solid curve. Three separate subcarriers are shown during three symbol intervals. In reality, an OFDM receiver only sees the sum of all these signals, but showing the separate components makes it more clear what the effect of multipath is. From the figure, we can see that the OFDM subcarriers are BPSK modulated, which means that there can be 180-degree phase jumps at the symbol boundaries. For the dotted curve, these phase jumps occur at a certain delay after the first path. In this particular example, this multipath delay is smaller than the guard time, which means there are no phase transitions during the FFT interval. Hence, an OFDM receiver "sees" the sum of pure sine waves with some phase offsets. This summation does not destroy the orthogonality between the subcarriers, it only introduces a different phase shift for each subcarrier. The orthogonality does become lost if the multipath delay becomes larger than the

:ounter some interference from the
there is no integer number of cycles
e time, there will be crosstalk from
1.

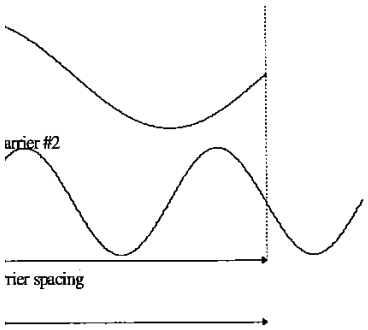

time; the delayed subcarrier 2 causes ICI on

lically extended in the guard time, as
plicas of the OFDM symbol always
T interval, as long as the delay is
signals with delays smaller than the

OFDM, Figure 2.8 shows received
irve is a delayed replica of the solid
three symbol intervals. In reality, an
signals, but showing the separate
of multipath is. From the figure, we
ilated, which means that there can be
s. For the dotted curve, these phase
ith. In this particular example, this
, which means there are no phase
DM receiver "sees" the sum of pure
on does not destroy the orthogonality
:rent phase shift for each subcarrier.
path delay becomes larger than the

guard time. In that case, the phase transitions of the delayed path fall within the FFT interval of the receiver. The summation of the sine waves of the first path with the phase modulated waves of the delayed path no longer gives a set of orthogonal pure sine waves, resulting in a certain level of interference.

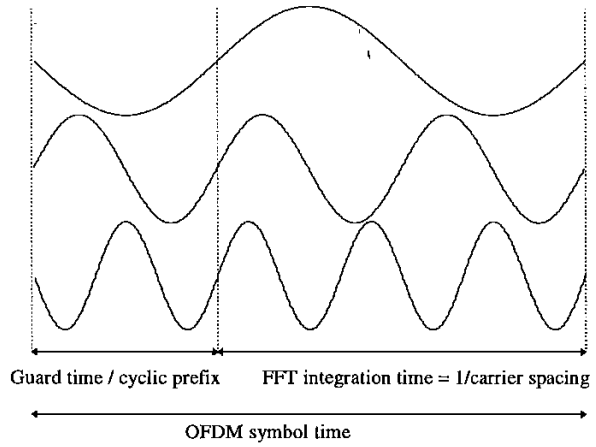

Figure 2.7 OFDM symbol with cyclic extension.

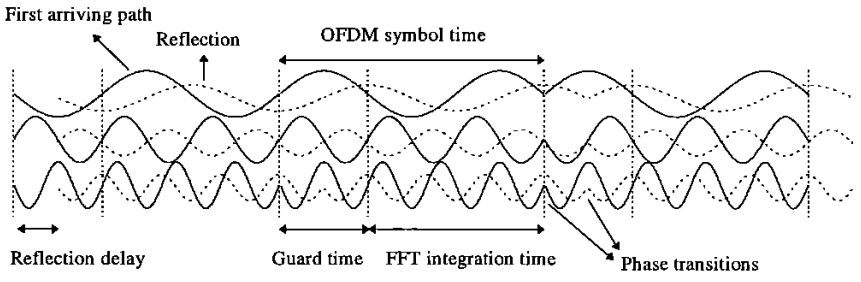

Figure 2.8 Example of an OFDM signal with three subcarriers in a two-ray multipath channel. The dashed line represents a delayed multipath component.

To get an idea what level of interference is introduced when the multipath delay exceeds the guard time, Figure 2.9 depicts three constellation diagrams that were derived from a simulation of an OFDM link with 48 subcarriers, each modulated by using 16-QAM. Figure 2.9(a) shows the undistorted 16-QAM constellation, which is observed whenever the multipath delay is below the guard time. In Figure 2.9(b), the multipath delay exceeds the guard time by a small 3% fraction of the FFT interval.

[redacted]

Hence, the subcarriers are not orthogonal anymore, but the interference is still small enough to get a reasonable received constellation. In Figure 2.9(c), the multipath delay exceeds the guard time by 10% of the FFT interval. The interference is now so large that the constellation is seriously blurred, causing an unacceptable error rate.

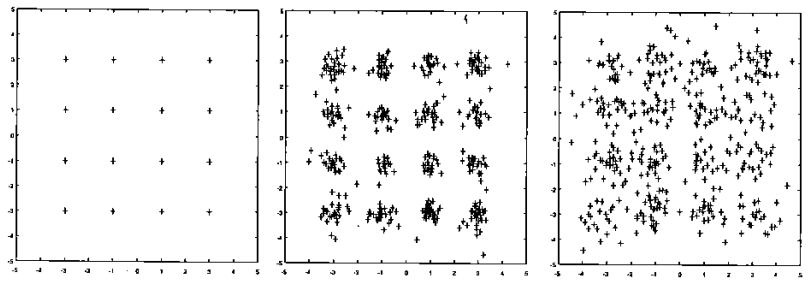

(a) (b) (c)

Figure 2.9 16-QAM constellation for a 48-subcarrier OFDM link with a two-ray multipath channel, the second ray being 6 dB lower than the first one. (a) delay < guard time; (b) delay exceeds guard time by 3% of the FFT interval; (c) delay exceeds guard time by 10% of the FFT interval.

2.4 WINDOWING

In the previous sections, it was explained how an OFDM symbol is formed by performing an IFFT and adding a cyclic extension. Looking at an example OFDM signal like in Figure 2.8, sharp phase transitions caused by the modulation can be seen at the symbol boundaries. Essentially, an OFDM signal like the one depicted in Figure 2.8 consists of a number of unfiltered QAM subcarriers. As a result, the out-of-band spectrum decreases rather slowly, according to a sinc function. As an example of this, the spectra for 16, 64, and 256 subcarriers are plotted in Figure 2.10. For larger number of subcarriers, the spectrum goes down more rapidly in the beginning, which is caused by the fact that the sidelobes are closer together. However, even the spectrum for 256 subcarriers has a relatively large –40-dB bandwidth that is almost four times the –3-dB bandwidth.

but the interference is still small
Figure 2.9(c), the multipath delay
The interference is now so large
nacceptable error rate.

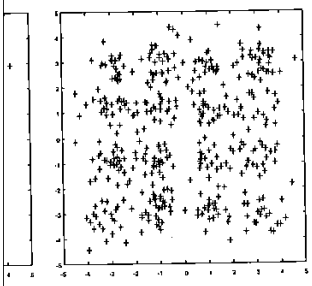

(c)

nk with a two-ray multipath channel, the
) delay < guard time; (b) delay exceeds
exceeds guard time by 10% of the FFT

n OFDM symbol is formed by
. Looking at an example OFDM
sed by the modulation can be seen
nal like the one depicted in Figure
riers. As a result, the out-of-band
c function. As an example of this,
l in Figure 2.10. For larger number
in the beginning, which is caused
owever, even the spectrum for 256
that is almost four times the –3-dB

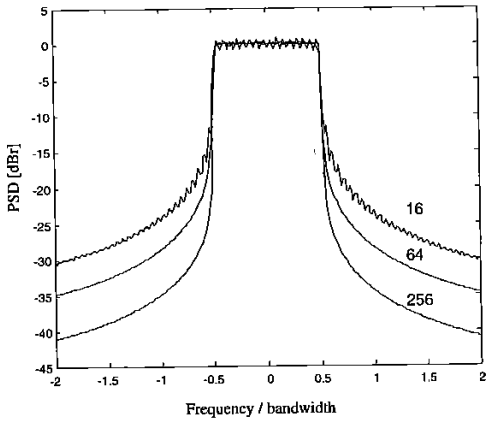

Figure 2.10 Power spectral density (PSD) without windowing for 16, 64, and 256 subcarriers.

To make the spectrum go down more rapidly, windowing can be applied to the individual OFDM symbols. Windowing an OFDM symbol makes the amplitude go smoothly to zero at the symbol boundaries. A commonly used window type is the raised cosine window, which is defined as

$$w(t)=\begin{cases} 0.5+0.5\cos\left(\pi+t\pi/(\beta T_s)\right) & 0 \le t \le \beta T_s \\ 1.0 & \beta T_s \le t \le T_s \\ 0.5+0.5\cos\left((t-T_s)\pi/(\beta T_s)\right) & T_s \le t \le (1+\beta)T_s \end{cases} \quad (2.6)$$

Here, T_s is the symbol interval, which is shorter than the total symbol duration because we allow adjacent symbols to partially overlap in the roll-off region. The time structure of the OFDM signal now looks like Figure 2.11.

In equation form, an OFDM symbol starting at time $t = t_s = kT_s$ is defined as

$$s_k(t)=\mathrm{Re}\left\{w(t-t_s)\sum_{i=-\frac{N_s}{2}}^{\frac{N_s}{2}-1} d_{i+N_s(k+1/2)}\exp\left(j2\pi\left(f_c-\frac{i+0.5}{T}\right)(t-t_s-T_{prefix})\right)\right\},\ t_s \le t \le t_s+T_s(1+\beta)$$

$$s_k(t)=0,\ t<t_s \wedge t>t_s+T_s(1+\beta) \quad (2.7)$$

In practice, the OFDM signal is generated as follows: first, N_c input QAM values are padded with zeros to get N input samples that are used to calculate an IFFT. Then, the last T_{prefix} samples of the IFFT output are inserted at the start of the OFDM symbol, and the first $T_{postfix}$ samples are appended at the end. The OFDM symbol is then multiplied by a raised cosine window $w(t)$ to more quickly reduce the power of out-of-band subcarriers. The OFDM symbol is then added to the output of the previous OFDM symbol with a delay of T_s, such that there is an overlap region of βT_s, where β is the rolloff factor of the raised cosine window.

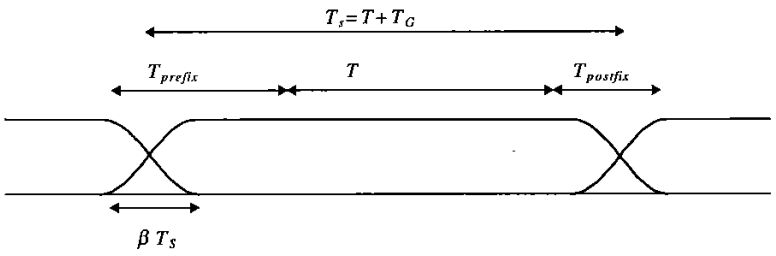

Figure 2.11 OFDM cyclic extension and windowing. T_s is the symbol time, T the FFT interval, T_G the guard time, T_{prefix} the preguard interval, $T_{postfix}$ the postguard interval, and β is the rolloff factor.

Figure 2.12 shows spectra for 64 subcarriers and different values of the rolloff factor β. It can be seen that a rolloff factor of 0.025—so the rolloff region is only 2.5% of the symbol interval—already makes a large improvement in the out-of-band spectrum. For instance, the –40-dB bandwidth is more than halved to about twice the –3-dB bandwidth. Larger rolloff factors improve the spectrum further, at the cost, however, of a decreased delay spread tolerance. The latter effect is demonstrated in Figure 2.13, which shows the signal structure of an OFDM signal for a two-ray multipath channel. The receiver demodulates the subcarriers by taking an FFT over the T-second interval between the dotted lines. Although the relative delay between the two multipath signals is smaller than the guard time, ICI and ISI are introduced because of the amplitude modulation in the gray part of the delayed OFDM symbol. The orthogonality between subcarriers as proved by (2.3) only holds when amplitude and phase of the subcarriers are constant during the entire T-second interval. Hence, a rolloff factor of β reduces the effective guard time by βT_s.

s follows: first, N_c input QAM
at are used to calculate an IFFT.
serted at the start of the OFDM
the end. The OFDM symbol is
ore quickly reduce the power of
ded to the output of the previous
n overlap region of βT_s, where β

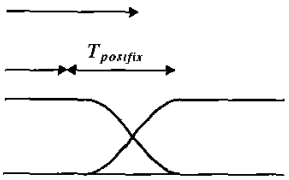

symbol time, T the FFT interval, T_G the
postguard interval, and β is the rolloff

and different values of the rolloff
-so the rolloff region is only 2.5%
mprovement in the out-of-band
re than halved to about twice the
he spectrum further, at the cost,
e latter effect is demonstrated in
an OFDM signal for a two-ray
carriers by taking an FFT over the
he relative delay between the two
and ISI are introduced because of
e delayed OFDM symbol. The
) only holds when amplitude and
tire T-second interval. Hence, a
βT_s.

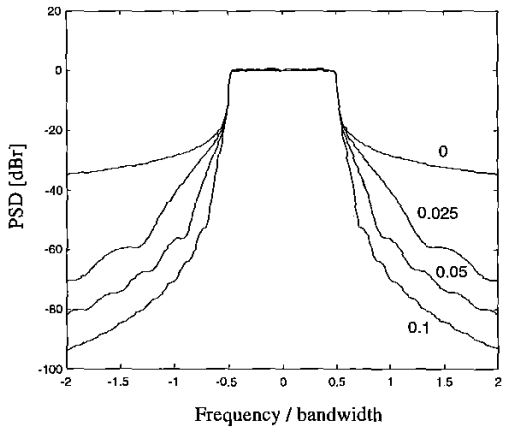

Figure 2.12 Spectra for raised cosine windowing with rolloff factors of 0 (rectangular window), 0.025, 0.05, and 0.1.

Instead of windowing, it is also possible to use conventional filtering techniques to reduce the out-of-band spectrum. Windowing and filtering are dual techniques; multiplying an OFDM symbol by a window means the spectrum is going to be a convolution of the spectrum of the window function with a set of impulses at the subcarrier frequencies. When filtering is applied, a convolution is done in the time domain and the OFDM spectrum is multiplied by the frequency response of the filter. When using filters, care has to be taken not to introduce rippling effects on the envelope of the OFDM symbols over a timespan that is larger than the rolloff region of the windowing approach. Too much rippling means the undistorted part of the OFDM envelope is smaller, and this directly translates into less delay spread tolerance. Notice that digital filtering techniques are more complex to implement than windowing. A digital filter requires at least a few multiplications per sample, while windowing only requires a few multiplications per symbol, for those samples which fall into the rolloff region. Hence, because only a few percent of the samples are in the rolloff region, windowing is an order of magnitude less complex than digital filtering.

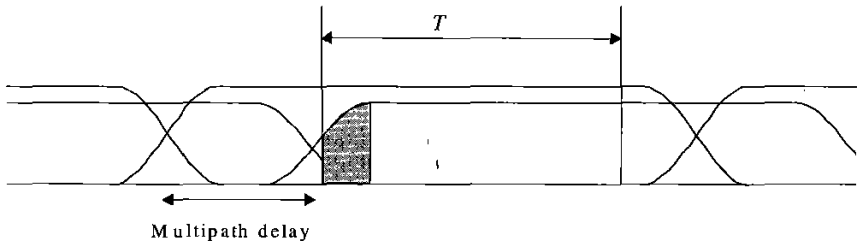

Figure 2.13 OFDM symbol windows for a two-ray multipath channel, showing ICI and ISI, because in the gray part, the amplitude of the delayed subcarriers is not constant.

2.5 CHOICE OF OFDM PARAMETERS

The choice of various OFDM parameters is a tradeoff between various, often conflicting requirements. Usually, there are three main requirements to start with: bandwidth, bit rate, and delay spread. The delay spread directly dictates the guard time. As a rule, the guard time should be about two to four times the root-mean-squared delay spread. This value depends on the type of coding and QAM modulation. Higher order QAM (like 64-QAM) is more sensitive to ICI and ISI than QPSK; while heavier coding obviously reduces the sensitivity to such interference.

Now that the guard time has been set, the symbol duration can be fixed. To minimize the signal-to-noise ratio (SNR) loss caused by the guard time, it is desirable to have the symbol duration much larger than the guard time. It cannot be arbitrarily large, however, because a larger symbol duration means more subcarriers with a smaller subcarrier spacing, a larger implementation complexity, and more sensitivity to phase noise and frequency offset [2], as well as an increased peak-to-average power ratio [3, 4]. Hence, a practical design choice is to make the symbol duration at least five times the guard time, which implies a 1-dB SNR loss because of the guard time.

After the symbol duration and guard time are fixed, the number of subcarriers follows directly as the required –3-dB bandwidth divided by the subcarrier spacing, which is the inverse of the symbol duration less the guard time. Alternatively, the number of subcarriers may be determined by the required bit rate divided by the bit rate per subcarrier. The bit rate per subcarrier is defined by the modulation type (e.g., 16-QAM), coding rate, and symbol rate.

As an example, suppose we want to design a system with the following requirements:

- Bit rate: 20 Mbps
- Tolerable delay spread: 200 ns
- Bandwidth: < 15 MHz

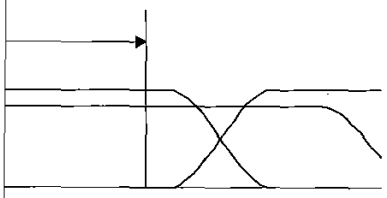

)ath channel, showing ICI and ISI, because in
bcarriers is not constant.

s a tradeoff between various, often
ree main requirements to start with:
spread directly dictates the guard time.
) to four times the root-mean-squared
coding and QAM modulation. Higher
ICI and ISI than QPSK; while heavier
interference.

the symbol duration can be fixed. To
aused by the guard time, it is desirable
the guard time. It cannot be arbitrarily
ation means more subcarriers with a
ion complexity, and more sensitivity to
as an increased peak-to-average power
) make the symbol duration at least five
loss because of the guard time.

ne are fixed, the number of subcarriers
dth divided by the subcarrier spacing,
ess the guard time. Alternatively, the
required bit rate divided by the bit rate
fined by the modulation type (e.g., 16-

design a system with the following

20 Mbps
200 ns
< 15 MHz

The delay-spread requirement of 200 ns suggests that 800 ns is a safe value for the guard time. By choosing the OFDM symbol duration 6 times the guard time (4.8 μs), the guard time loss is made smaller than 1 dB. The subcarrier spacing is now the inverse of 4.8 – 0.8 = 4 μs, which gives 250 kHz. To determine the number of subcarriers needed, we can look at the ratio of the required bit rate and the OFDM symbol rate. To achieve 20 Mbps, each OFDM symbol has to carry 96 bits of information (96/4.8 μs = 20 Mbps). To do this, there are several options. One is to use 16-QAM together with rate ½ coding to get 2 bits per symbol per subcarrier. In this case, 48 subcarriers are needed to get the required 96 bits per symbol. Another option is to use QPSK with rate ¾ coding, which gives 1.5 bits per symbol per subcarrier. In this case, 64 subcarriers are needed to reach the 96 bits per symbol. However, 64 subcarriers means a bandwidth of 64·250 kHz = 16 MHz, which is larger than the target bandwidth. To achieve a bandwidth smaller than 15 MHz, the number of subcarriers needs to be smaller than 60. Hence, the first option with 48 subcarriers and 16-QAM fulfills all the requirements. It has the additional advantage that an efficient 64-point radix-4 FFT/IFFT can be used, leaving 16 zero subcarriers to provide oversampling necessary to avoid aliasing.

An additional requirement that can affect the chosen parameters is the demand for an integer number of samples both within the FFT/IFFT interval and in the symbol interval. For instance, in the above example we want to have exactly 64 samples in the FFT/IFFT interval to preserve orthogonality among the subcarriers. This can be achieved by making the sampling rate 64/4 μs = 16 MHz. However, for that particular sampling rate, there is no integer number of samples with the symbol interval of 4.8 μs. The only solution to this problem is to change one of the parameters slightly to meet the integer constraint. For instance, the number of samples per symbol can be set to 78, which gives a sampling rate of 78/4.8 μs = 16.25 MHz. Now, the FFT interval becomes 64/16.25 MHz = 3.9385 μs, so both guard time and subcarrier spacing are slightly larger than in the case of the original FFT interval of 4 μs.

2.6 OFDM SIGNAL PROCESSING

The previous sections described how the basic OFDM signal is formed using the IFFT, adding a cyclic extension and performing windowing to get a steeper spectral rolloff. However, there is more to it to build a complete OFDM modem. Figure 2.14 shows the block diagram of an OFDM modem, where the upper path is the transmitter chain and the lower path corresponds to the receiver chain. In the center we see the IFFT, which modulates a block of input QAM values onto a number of subcarriers. In the receiver, the subcarriers are demodulated by an FFT, which performs the reverse operation of an IFFT. An interesting feature of the FFT/IFFT is that the FFT is almost identical to an IFFT. In fact, an IFFT can be made using an FFT by conjugating input and output of the FFT and dividing the output by the FFT size. This makes it possible to use the same hardware for both transmitter and receiver. Of course, this saving in complexity is only possible when the modem does not have to transmit and receive simultaneously.

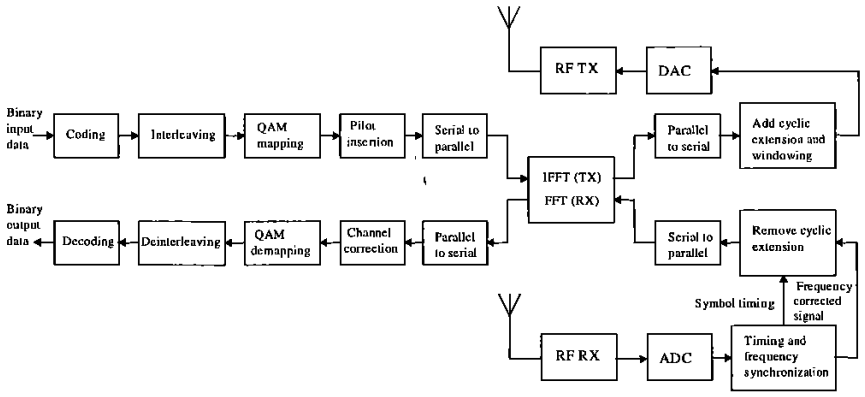

Figure 2.14 Block diagram of an OFDM transceiver.

The functions before the IFFT have not been discussed till now. Binary input data is first encoded by a forward error correction code. The encoded data is then interleaved and mapped onto QAM values. These functions are discussed in more detail in the next chapter.

In the receiver path, after passing the RF part and the analog-to-digital conversion, the digital signal processing starts with a training phase to determine symbol timing and frequency offset. An FFT is used to demodulate all subcarriers. The output of the FFT contains N_s QAM values, which are mapped onto binary values and decoded to produce binary output data. To successfully map the QAM values onto binary values, first the reference phases and amplitudes of all subcarriers have to be acquired. Alternatively, differential techniques can be applied. All of these receiver functions are highlighted in the following chapters.

2.7 IMPLEMENTATION COMPLEXITY OF OFDM VERSUS SINGLE-CARRIER MODULATION

One of the main reasons to use OFDM is its ability to deal with large delay spreads with a reasonable implementation complexity. In a single-carrier system, the implementation complexity is dominated by equalization, which is necessary when the delay spread is larger than about 10% of the symbol duration. OFDM does not require an equalizer. Instead, the complexity of an OFDM system is largely determined by the FFT, which is used to demodulate the various subcarriers. In the following example, it is demonstrated that the processing complexity of an OFDM modem can be significantly less than that of a single carrier modem, given the fact that both can deal with the same amount of delay spread. Notice that some papers mention the use of a

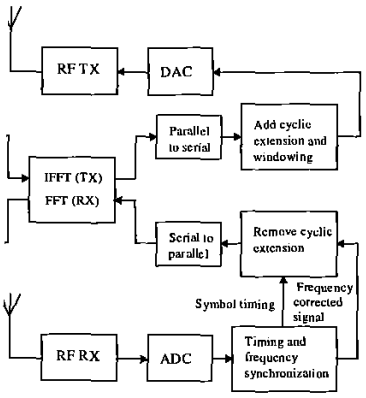

)FDM transceiver.

een discussed till now. Binary input on code. The encoded data is then unctions are discussed in more detail

RF part and the analog-to-digital with a training phase to determine ed to demodulate all subcarriers. The n are mapped onto binary values and essfully map the QAM values onto litudes of all subcarriers have to be an be applied. All of these receiver

)F OFDM VERSUS

lity to deal with large delay spreads . In a single-carrier system, the ization, which is necessary when the ol duration. OFDM does not require system is largely determined by the carriers. In the following example, it ty of an OFDM modem can be em, given the fact that both can deal at some papers mention the use of a

single-tap equalizer for OFDM, when they are referring to the phase correction in case of a coherent OFDM receiver. We will not use this somewhat confusing terminology, because the term equalization suggests that an attempt is made to invert the channel, while an OFDM receiver is doing the opposite; weak subcarriers are not being extra amplified to equalize the channel, but rather, they get a low weight in the decoding. In this way, OFDM avoids the problem of noise enhancement that is present in linear equalization techniques.

Figure 2.15 shows the block diagram of a decision feedback equalizer with symbol-spaced taps. Such an equalizer can be used to combat delay spread in single-carrier systems using quadrature amplitude modulation (QAM) or some form of constant amplitude modulation such as Gaussian Minimum Shift Keying (GMSK) or offset-QPSK. From references [5, 6], it can be learned that at least 8 feedforward and 8 feedback taps are required to handle a delay spread of 100 ns for a GMSK modem at a data rate of 24 Mbps. We can use this information to compare a single carrier system with the 24 Mbps mode of the new IEEE 802.11 OFDM standard, which can handle delay spreads up to 250 ns using a 64-point FFT. In order to increase the delay spread tolerance of a GMSK modem to the same level, the equalizer length has to be increased by a factor of 250/100, so it has 20 feedforward and feedback taps. Fortunately, for GMSK only the real outputs of the complex multiplications are used, so each multiplier has to perform two real multiplications per sample. Hence, the number of real multiplications per second becomes $2 \cdot 20 \cdot 24 \cdot 10^6 = 960 \cdot 10^6$. Notice we only count the feedforward taps here, since the feedback taps consist of trivial rotations, while the feedforward taps consist of full multiplications. For the OFDM system, a 64-point FFT has to be processed by every OFDM symbol duration which is 4 μs, see chapter 10. With a radix-4 algorithm, this requires 96 complex multiplications [1], which gives a processing load of $96 \cdot 10^6$ real multiplications per second. So, in terms of multiplications per second, the equalizer of the single carrier system is 10 times more complex than the FFT of the OFDM system! This complexity difference grows with the bit rate, or rather with the bandwidth – delay spread product, which is a measure of the relative amount of inter-symbol interference. For instance, if we want to double the bit rate in the previous example by doubling the bandwidth, but the delay spread tolerance has to stay the same, then the number of subcarriers and the guard time has to be doubled for OFDM, while for the single-carrier system, both the number of equalizer taps and the sampling rate are doubled. The latter means that the number of multiplications per second is quadrupled, so the equalizer complexity grows quadratically with the bandwidth – delay spread product. For OFDM, a double-sized FFT has to be calculated in the same amount of time in order to double the rate. For the radix-2 algorithm, this means an increase in the number of multiplications of $N\log_2(2N)/\ (N/2)\log_2 N = 2(1+1/\log_2 N)$, where N is the FFT size for the half-rate system. The complexity of the FFT grows only slightly faster than linear with the bandwidth – delay spread product, which explains why OFDM is more attractive than a single carrier system with equalization for relatively large bandwidth – delay spread products (values around 1 or larger). It should be noted that the complexity difference between the FFT and the equalizer is less if the equalization is done in the frequency domain, as

described in [7]. In this case, equalization is twice as complex, because both an FFT and an IFFT have to be performed to do frequency domain equalization on a signal block.

Another complexity advantage of OFDM is the fact that the FFT does not really require full multiplications, but rather phase rotations, which can be efficiently implemented by the CORDIC algorithm [8]. Because phase rotations do not change the amplitude, they do not increase the dynamic range of the signals, which simplifies the fixed point design.

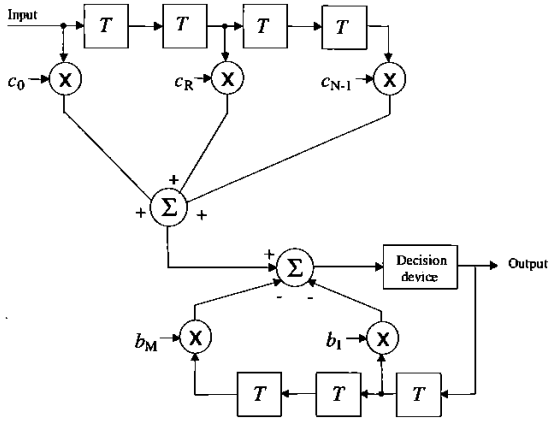

Figure 2.15 Decision-feedback equalizer.

Except for the difference in complexity, OFDM has another advantage over single carrier systems with equalizers. For the latter systems, the performance degrades abruptly if the delay spread exceeds the value for which the equalizer is designed. Because of error propagation, the raw bit error probability increases so quickly that inroducing lower rate coding or a lower constellation size does not significantly improve the delay spread robustness. For OFDM, however, there are no such nonlinear effects as error propagation, and coding and lower constellation sizes can be employed to provide fallback rates that are significantly more robust against delay spread. This is an important consideration, as it enhances the coverage area and avoids the situation that users in bad spots cannot get any connection at all.

ce as complex, because both an FFT
ncy domain equalization on a signal

is the fact that the FFT does not really
rotations, which can be efficiently
ause phase rotations do not change the
ge of the signals, which simplifies the

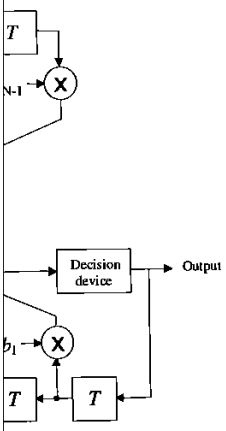

back equalizer.

, OFDM has another advantage over
tter systems, the performance degrades
for which the equalizer is designed.
r probability increases so quickly that
nstellation size does not significantly
I, however, there are no such nonlinear
ver constellation sizes can be employed
ore robust against delay spread. This is
coverage area and avoids the situation
n at all.

REFERENCES

[1] Blahut, R. E., *Fast Algorithms for Digital Signal Processing*. Reading, MA: Addison-Wesley, 1985.

[2] Pollet, T., M. van Bladel and M. Moeneclaey, "BER Sensitivity of OFDM Systems to Carrier Frequency Offset and Wiener Phase Noise," *IEEE Trans. on Comm.*, Vol. 43, No. 2/3/4, pp. 191–193, Feb.–Apr. 1995.

[3] Pauli, M., and H. P. Kuchenbecker, "Minimization of the Intermodulation Distortion of a Nonlinearly Amplified OFDM Signal," *Wireless Personal Communications*, Vol. 4, No. 1, pp. 93–101, Jan. 1997.

[4] Rapp, C., "Effects of HPA-Nonlinearity on a 4-DPSK/OFDM Signal for a Digital Sound Broadcasting System," *Proc. of the Second European Conference on Satellite Communications*, Liège, Belgium, pp.179–184, Oct. 22–24, 1991.

[5] Tellado-Mourelo, J., E. K.Wesel, J. M.Cioffi, "Adaptive DFE for GMSK in Indoor Radio Channels," *IEEE Trans. on Sel. Areas in Comm.*, Vol. 14, No. 3, pp. 492–501, Apr. 1996.

[6] Wales, S. W., "Modulation and Equalization Techniques for HIPERLAN," *Proc. of PIMRC/WCN*, The Hague, The Netherlands, Sept. 21–23, pp. 959–963, 1994.

[7] Sari, H., G. Karam, I. Jeanclaude, "Transmission Techniques for Digital Terrestrial TV Broadcasting," *IEEE Communications Magazine*, Feb. 1995, pp. 100–109.

[8] Parhi, K. K., and T. Nishitani, *Digital Signal Processing for Multimedia Systems*. New York: Marcel Dekker, Inc., 1999.

Chapter 3

Coding and Modulation

3.1 INTRODUCTION

We explained in the previous chapter how OFDM avoids the problem of intersymbol interference by transmitting a number of narrowband subcarriers together with using a guard time. This does give rise to another problem, however, which is the fact that in a multipath fading channel, all subcarriers will arrive at the receiver with different amplitudes. In fact, some subcarriers may be completely lost because of deep fades. Hence, even though most subcarriers may be detected without errors, the overall bit-error ratio (BER) will be largely dominated by a few subcarriers with the smallest amplitudes, for which the bit-error probability is close to 0.5. To avoid this domination by the weakest subcarriers, forward-error correction coding is essential. By using coding across the subcarriers, errors of weak subcarriers can be corrected up to a certain limit that depends on the code and the channel. A powerful coding means that the performance of an OFDM link is determined by the average received power, rather than by the power of the weakest subcarrier.

This chapter starts with a review of block codes and convolutional codes. Then, it introduces interleaving as a way to randomize error bursts that occur when adjacent subcarriers are lost in a deep fade. Section 3.4 describes QAM as the most commonly used modulation technique in OFDM, after which Section 3.5 shows the important relation between coding and modulation. Thus, this chapter presents a brief overview of coding and modulation [1–9].

3.2 FORWARD-ERROR CORRECTION CODING

3.2.1 Block Codes

A *block code* encodes a block of k input symbols into n coded symbols, with n being larger than k. The purpose of adding the redundant n-k symbols is to increase the *minimum Hamming distance*, which is the minimum number of different symbols between any pair of code words. For a minimum Hamming distance of d_{min}, the code can correct t errors where t is given by

$$t \leq floor(\frac{d_{\min}-1}{2}) \tag{3.1}$$

Here, *floor(x)* denotes the floor function that rounds x downward to the closest integer value. The minimum Hamming distance is upperbound by the number of redundant symbols n-k as

$$d_{\min} \leq n-k+1 \tag{3.2}$$

For binary codes, only repetition codes and single-parity check codes reach this upperbound. A class of nonbinary codes that does reach the above bound are the *Reed-Solomon codes*. Because of their good distance properties and the availabity of efficient coding and decoding algorithms [6, 7], Reed-Solomon codes are the most popularly used block codes. Reed-Solomon codes are defined for blocks of symbols with m bits per symbol, where the code length n is related to m by

$$n = 2^m - 1 \tag{3.3}$$

The number of input symbols k is related to m and the required minimum Hamming distance d_{min} as

$$k = 2^m - d_{\min} \tag{3.4}$$

There appears to be little flexibility in the available code lengths as indicated by (3.3). However, a Reed-Solomon code can easily be shortened to any arbitrary length

by leaving a number of input bits zero and deleting the same amount of output bits. It is also possible to extend the code length to a power of 2 by adding an extra parity symbol.

According to (3.1) and (3.2), a Reed-Solomon code can correct up to floor((*n*-*k*)/2) erroneous symbols. Each symbol contains *m* bits, so a maximum amount of *m*·floor((*n*-*k*)/2) erroneous bits may be corrected. The latter is only true, however, if all bit errors occur within the maximum amount of correctable symbol errors. So if a Reed-Solomon is designed to correct up to two symbol errors containing 8 bits per symbol, it cannot correct an arbitrary combination of three bit errors, as these errors may occur in three different symbols. This characteristic makes Reed-Solomon codes particularly useful for correcting bursty channels. One example of such a channel is an OFDM link in the presence of multipath fading, which causes the errors to be concentrated in a few subcarriers that are hit by deep fades.

3.2.2 Convolutional Codes

A convolutional code maps each *k* bits of a continuous input stream on *n* output bits, where the mapping is performed by convolving the input bits with a binary impulse response. The convolutional encoding can be implemented by simple shift registers and modulo-2 adders. As an example, Figure 3.1 shows the encoder for a rate 1/2 code which is actually one of the most frequently applied convolutional codes. This encoder has a single data input and two outputs A_i and B_i, which are interleaved to form the coded output sequence $\{A_1B_1A_2B_2 \ldots\}$. Each pair of output bits $\{A_i,B_i\}$ depends on seven input bits, being the current input bit plus six previous input bits that are stored in the length 6 shift register. This value of 7—or in general the shift register length plus 1—is called the *constraint length*. The shift register taps are often specified by the corresponding generator polynomials or generator vectors. For the example of Figure 3.1, the generator vectors are {1011011,1111001} or {133,171} octal. The ones in the generator vectors correspond with taps on the shift register.

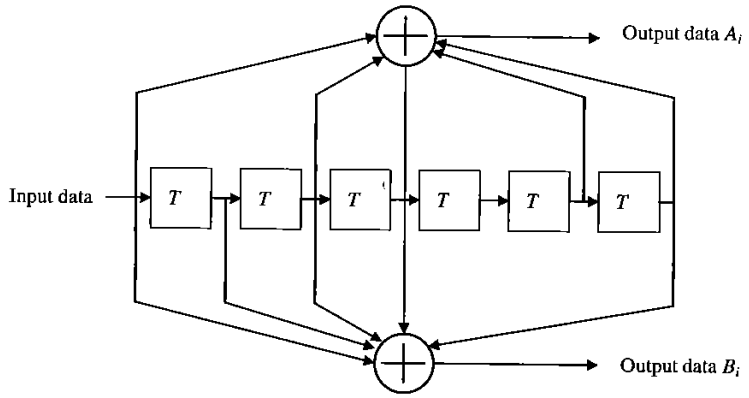

Figure 3.1 Block diagram of a constraint length 7 convolutional encoder.

Decoding of convolutional codes is most often performed by *soft decision Viterbi decoding*, which is an efficient way to obtain the optimal maximum likelihood estimate of the encoded sequence. A description of this decoding technique can be found in [8]. The complexity of Viterbi decoding grows exponentially with the constraint length. Hence, practical implementations do not go further than a constraint length of about 10. Decoding of convolutional codes with larger constraint length is possible by using suboptimal decoding techniques like sequential decoding [8].

Because convolutional codes do not have a fixed length, it is more difficult to specify their performance in terms of Hamming distance and a number of correctable errors. One measure that is used is the *free distance*, which is the minimum Hamming distance between arbitrarily long different code sequences that begin and end with the same state of the encoder, where the state is defined by the contents of the shift registers of the encoder. For example, the code of Figure 3.1 has a free distance of 10. When hard decision decoding is used, this code can correct up to floor((10-1)/2) = 4 bit errors within each group of encoded bits with a length of about 3 to 5 times the constraint length. When soft decision decoding is used, however, the number of correctable errors does not really give a useful measure anymore. A better performance measure is the *coding gain*, which is defined as the gain in the bit energy-to-noise density ratio E_b/N_o relative to an uncoded system to achieve a certain bit error ratio. The E_b/N_o gain is equivalent to the gain in input signal-to-noise ratio (SNR) minus the rate loss in dB because of the redundant bits. As an example, Figure 3.2 shows the bit error ratio versus E_b/N_o for uncoded QPSK and for coded QPSK using the previously mentioned constraint length 7 code. It can be seen from the figure that for a bit-error ratio of 10^{-4}, the coded link needs about 5 dB less E_b/N_o compared with that of the uncoded link. For lower bit error ratios, this coding gain converges to a maximum value of about 5.5 dB.

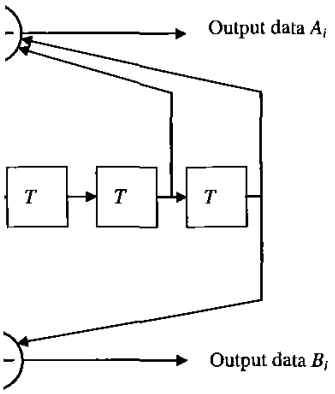

length 7 convolutional encoder.

ıost often performed by *soft decision* ɔbtain the optimal maximum likelihood ion of this decoding technique can be coding grows exponentially with the ions do not go further than a constraint l codes with larger constraint length is es like sequential decoding [8].

ve a fixed length, it is more difficult to g distance and a number of correctable *tance*, which is the minimum Hamming ; sequences that begin and end with the s defined by the contents of the shift of Figure 3.1 has a free distance of 10. can correct up to floor((10-1)/2) = 4 bit h a length of about 3 to 5 times the ing is used, however, the number of measure anymore. A better performance as the gain in the bit energy-to-noise n to achieve a certain bit error ratio. The ;nal-to-noise ratio (SNR) minus the rate example, Figure 3.2 shows the bit error or coded QPSK using the previously seen from the figure that for a bit-error 3 less E_b/N_o compared with that of the ing gain converges to a maximum value

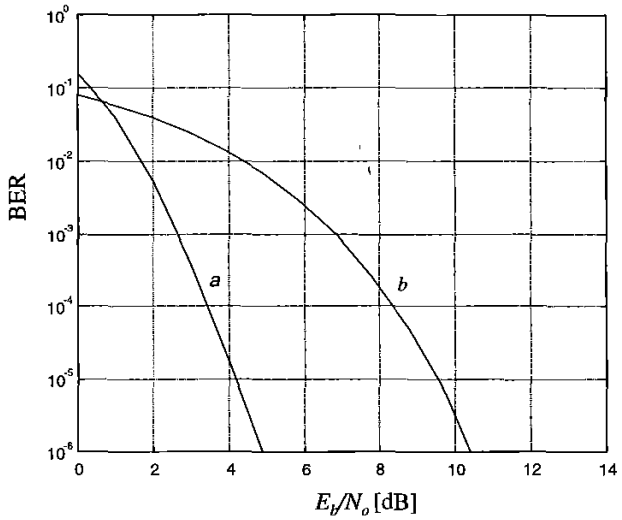

Figure 3.2 BER versus E_b/N_o for coded and uncoded QPSK in AWGN.

In the above curves, we have used the bit energy-to-noise density ratio E_b/N_o, which is equivalent to the ratio of the signal power P and the noise power in a bandwidth equal to the bit rate N_o/T_b, where T_b is the bit time. Some other useful SNR definitions are the input SNR and the symbol energy-to-noise density ratio E_s/N_o, which is equivalent to the ratio of the signal power and the noise power within a bandwidth equal to the symbol rate N_o/T_s, where T_s is the symbol duration. E_s/N_o is equivalent to the SNR for individual subcarriers, plus the guard time loss in dB. It is related to E_b/N_o as

$$\frac{E_s}{N_o} = \frac{E_b}{N_o}\frac{T_s}{T_b} \tag{3.5}$$

The input signal-to-noise ratio SNR_i is related to E_b/N_o as

$$SNR_i = \frac{E_b}{N_o}\frac{1}{BT_b} = \frac{E_b}{N_o}\frac{bN_s r}{BT_s} \tag{3.6}$$

Here, B is the input noise bandwidth, b is the number of coded bits per subcarrier, N_s the number of subcarriers, and r the coding rate. Basically, the SNR_i is equal to E_b/N_o multiplied by the ratio of bit rate and bandwidth. The latter ratio is equivalent to the spectral efficiency in bps/Hz. The spectral efficiency depends on the number of bits per subcarrier b, which is determined by the constellation size, the coding rate r, and the guard time, which appears indirectly in (3.6) as a part of the

symbol duration T_s. The number of subcarriers has no influence on the spectral efficiency, because the noise bandwidth increases linearly with the number of subcarriers.

A convolutional code can be punctured to increase the coding rate. For instance, increasing the rate of the above rate 1/2 code to 3/4 is done by deleting 2 of every 6 bits at the output of the encoder. The punctured output sequence for a rate 3/4 code is $\{A_1B_1A_2B_3A_4B_4A_5B_6A_7B_7 \ldots\}$. For a rate 2/3 code, the punctured output sequence is $\{A_1B_1A_2A_3B_3A_4A_5B_5 \ldots\}$. To decode the punctured sequence, the original rate 1/2 decoder can be used. Before decoding, erasures have to be inserted in the data at the locations of the punctured bits.

3.2.3 Concatenated Codes

Instead of using a single block code or convolutional code, it is also possible to combine or concatenate two codes. The main advantage of a concatenated code is that it can provide a large coding gain with less implementation complexity as a comparable single code. Figure 3.3 shows the block diagram of a concatenated coding scheme. The input bits are first coded and interleaved by an outer coder and interleaver. The coded bits are then again coded and interleaved by an inner coder and interleaver. Usually, the inner code is a convolutional code and the outer code a block code; for instance, a Reed-Solomon code. The motivation behind this is that the convolutional code with soft decision decoding performs better for relatively low-input SNRs. The hard decision block decoder then cleans up the relatively few remaining errors in the decoded output bits of the convolutional decoder. The task of the interleavers is to break up bursts of errors as much as possible. In case of an outer block code, the outer interleaver preferably separates symbols by more than the block length of the outer encoder. Compared with a single-code system, concatenated coding has more delay because of the extra interleaving, which can be a disadvantage for packet communications where the interleaving delay affects turnaround time and throughput. A good overview of achievable performance of concatenated coding is given in [3].

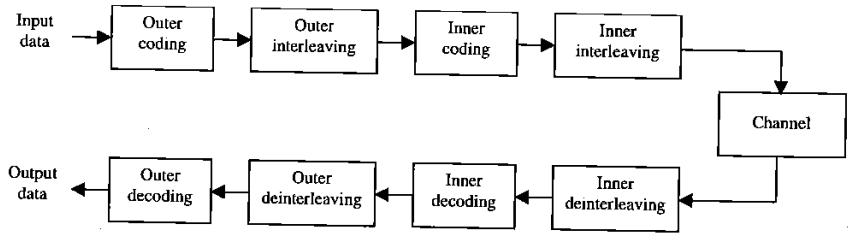

Figure 3.3 Concatenated coding/decoding.

rs has no influence on the spectral
eases linearly with the number of

increase the coding rate. For instance,
/4 is done by deleting 2 of every 6 bits
itput sequence for a rate 3/4 code is
de, the punctured output sequence is
ured sequence, the original rate 1/2
have to be inserted in the data at the

olutional code, it is also possible to
vantage of a concatenated code is that
mentation complexity as a comparable
of a concatenated coding scheme. The
outer coder and interleaver. The coded
ner coder and interleaver. Usually, the
er code a block code; for instance, a
is is that the convolutional code with
ely low-input SNRs. The hard decision
emaining errors in the decoded output
ie interleavers is to break up bursts of
ter block code, the outer interleaver
e block length of the outer encoder.
ted coding has more delay because of
age for packet communications where
and throughput. A good overview of
s given in [3].

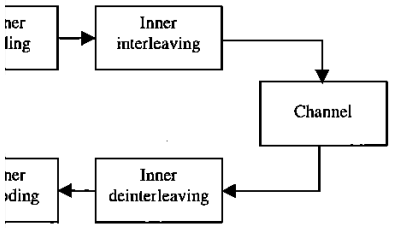

oding/decoding.

3.3 INTERLEAVING

Because of the frequency selective fading of typical radio channels, the OFDM subcarriers generally have different amplitudes. Deep fades in the frequency spectrum may cause groups of subcarriers to be less reliable than others, thereby causing bit errors to occur in bursts rather than being randomly scattered. Most forward error-correction codes are not designed to deal with error bursts. Therefore, interleaving is applied to randomize the occurrence of bit errors prior to decoding. At the transmitter, the coded bits are permuted in a certain way, which makes sure that adjacent bits are separated by several bits after interleaving. At the receiver, the reverse permutation is performed before decoding. A commonly used interleaving scheme is the block interleaver, where input bits are written in a matrix column by column and read out row by row. As an example of such an interleaver, Figure 3.4 shows the bit numbers of a block interleaver operating on a block size of 48 bits. After writing the 48 bits in the matrix according to the order as depicted in the figure, the interleaved bits are read out row by row, so the output bit numbers are 0, 8, 16, 24, 32, 40, 1, 9, . . . , 47. Instead of bits, the operation can also be applied on symbols; for instance, the matrix can be filled with 48 16-QAM symbols containing 4 bits per symbol, so the interleaving changes the symbol order but not the bit order within each symbol. Interleaving on a symbol-basis is especially useful for Reed-Solomon codes, as these codes operate on symbols rather than bits. A Reed-Solomon code can correct up to a certain number of symbol errors per block length, so interleaving should be done over several block lengths, in order to spread bursts of symbol errors over a number of different Reed-Solomon blocks.

0	8	16	24	32	40
1	9	17	25	33	41
2	10	18	26	34	42
3	11	19	27	35	43
4	12	20	28	36	44
5	13	21	29	37	45
6	14	22	30	38	46
7	15	23	31	39	47

Figure 3.4 Interleaving scheme.

For a general block interleaver with a block size of N_B bits and d columns, the ith interleaved bit is equal to the kth encoded input bit, where k is given by

$$k = id - (N_B - 1)\,floor(\frac{id}{N_B}) \tag{3.7}$$

Instead of a block interleaver, it is also possible to use a convolutional interleaver. An example of this type of interleaver is shown in Figure 3.5. The interleaver cyclically writes each input symbol or bit into one of K shift registers that introduce a delay of 0 to k-1 symbol durations. The shift registers are read out cyclically to produce the interleaved symbols.

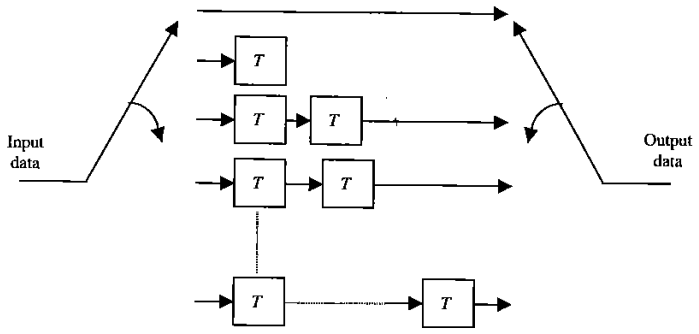

Figure 3.5 Convolutional interleaver.

3.4 QUADRATURE AMPLITUDE MODULATION

Quadrature amplitude modulation (QAM) is the most popular type of modulation in combination with OFDM. Especially rectangular constellations are easy to implement as they can be split into independent *Pulse amplitude modulated* (PAM) components for both the in-phase and the quadrature part. Figure 3.6 shows the rectangular constellations of Quadrature Phase Shift Keying (QPSK), 16-QAM, and 64-QAM. The constellations are not normalized; to normalize them to an average power of one—assuming that all constellation points are equally likely to occur—each constellation has to be multiplied by the normalization factor listed in Table 3.1. The table also mentions Binary Phase Shift Keying (BPSK), which uses two of the four QPSK constellation points (1+j, –1–j).

Table 3.1 also gives the loss in the minimum squared Euclidean distance between two constellation points, divided by the gain in data rate of that particular QAM type relative to BPSK. This value defines the maximum loss in E_b/N_o relative to BPSK that is needed to achieve a certain bit-error ratio in an uncoded QAM link. The BER curves in Figure 3.7 illustrate that the E_b/N_o loss values of Table 3.1 are quite accurate for BER values below 10^{-2}. The difference between QPSK and 16-QAM is about 4 dB. From 16-QAM to 64-QAM, almost 4.5 dB extra E_b/N_o is required. For larger constellation sizes, the E_b/N_o penalty of increasing the number of bits per symbol by 1 converges to 3 dB.

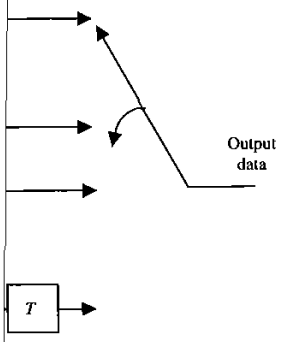

terleaver.

ATION

most popular type of modulation in constellations are easy to implement *tude modulated* (PAM) components Figure 3.6 shows the rectangular QPSK), 16-QAM, and 64-QAM. The hem to an average power of one— likely to occur—each constellation listed in Table 3.1. The table also which uses two of the four QPSK

nimum squared Euclidean distance gain in data rate of that particular e maximum loss in E_b/N_o relative to ratio in an uncoded QAM link. The loss values of Table 3.1 are quite ice between QPSK and 16-QAM is 4.5 dB extra E_b/N_o is required. For asing the number of bits per symbol

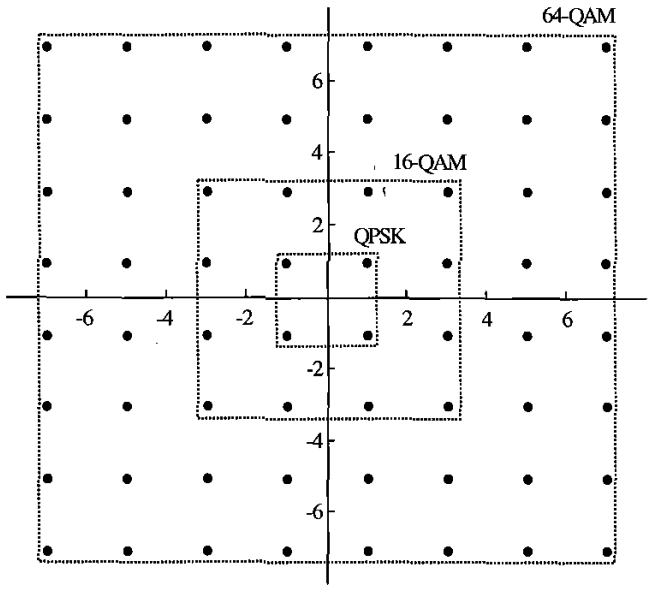

Figure 3.6 QPSK, 16-QAM, and 64-QAM constellations.

Table 3.1
QAM normalization factors and normalized Euclidean distance differences.

Modulation	Normalization factor	Maximum E_b/N_o loss relative to BPSK in dB
BPSK	$1/\sqrt{2}$	0
QPSK	$1/\sqrt{2}$	0
16-QAM	$1/\sqrt{10}$	3.98
64-QAM	$1/\sqrt{42}$	8.45

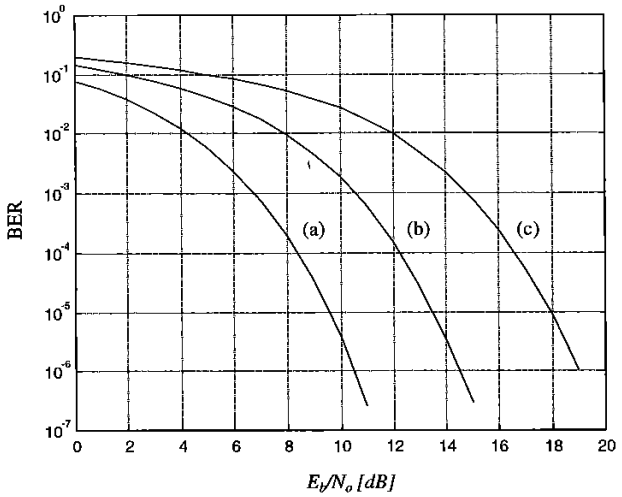

Figure 3.7 BER versus E_b/N_o for (a) BPSK/QPSK, (b) 16-QAM, (c) 64-QAM.

3.5 CODED MODULATION

When coding is applied to a QAM signal, it is important to consider the relation between coding and modulation to obtain the best result. In [9], Trellis coding was introduced as a way to attain coding gain without bandwidth expansion, meaning that all redundancy is obtained by increasing the constellation size. It was demonstrated in [9] that coding gains up to 6 dB can be obtained by going from uncoded QPSK to Trellis-coded 8-PSK using rate 2/3 coding. This technique is based on partitioning the PSK or QAM constellations into subsets with a high Euclidean distance within each subset. For instance, each 2 8-PSK constellation points with a relative phase difference of 180° define a subset with the same Euclidean distance as BPSK. The minimum Euclidean distance between different subsets is much smaller. Hence, coding is applied on the bits defining the subset number, such that the minimum Euclidean distance of the coded signal becomes equal to the distance within each subset.

A disadvantage of the above Trellis coding approach is that although the codes can have a large minimum Euclidean distance, the minimum Hamming distance is only 1, because bits within a subset are left uncoded. Hence, if one Trellis-coded symbol is lost, this immediately results in one or more bit errors. For OFDM this is a very undesirable property, as the data of several subcarriers may be lost by deep fades. This illustrates that the minimum Euclidean distance is not the only relevant parameter when selecting a good code for OFDM. For frequency selective channels, an additional criterion is that the Euclidean distance should be spread over as many symbols as possible, such that a few lost symbols have the smallest possible impact on the

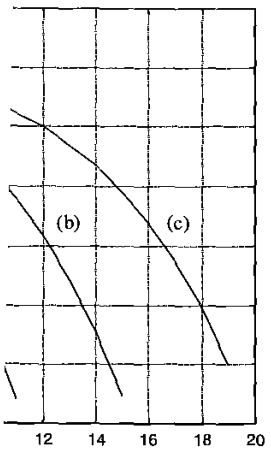

PSK, (b) 16-QAM, (c) 64-QAM.

is important to consider the relation
best result. In [9], Trellis coding was
ut bandwidth expansion, meaning that
stellation size. It was demonstrated in
ied by going from uncoded QPSK to
technique is based on partitioning the
a high Euclidean distance within each
points with a relative phase difference
an distance as BPSK. The minimum
nuch smaller. Hence, coding is applied
at the minimum Euclidean distance of
ithin each subset.

ng approach is that although the codes
ie minimum Hamming distance is only
Hence, if one Trellis-coded symbol is
bit errors. For OFDM this is a very
arriers may be lost by deep fades. This
s not the only relevant parameter when
ncy selective channels, an additional
be spread over as many symbols as
the smallest possible impact on the

probability of a decoding error [1]. As a consequence, in fading channels it is preferable to use high-order QAM constellations in combination with low-rate coding schemes. It is demonstrated in [1] that a specially designed rate 1/4 code with constraint length 7 together with a 16-QAM constellation can give good performance even on channels where more than half of the subcarriers are lost, with a degradation of less than 2 dB in the required signal-to-noise ratio relative to an ideal AWGN channel.

One of the disadvantages of special Trellis codes is that they are designed for specific constellations, such that you need a different encoder and decoder for different constellations. A practical approach to avoid this problem is to use standard binary codes together with Gray-encoded QAM. In [4], for instance, an efficient way is described to use a standard binary convolutional code together with 16-QAM. This scheme can easily be extended to an arbitrary rectangular QAM constellation. To do this, binary input data are converted into QAM symbols according to a Gray code mapping. For 16-QAM, for instance, the in-phase and quadrature parts are separately formed as 4 level PAM values, determined by two bits $b0$ and $b1$, as shown in Figure 3.8. The vertical lines indicate the regions for which the bit values are 1.

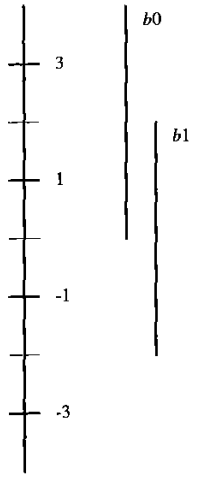

Figure 3.8 Gray mapping of two bits into 4 level PAM.

In the receiver, the incoming QAM symbols have to be demapped into one-dimensional values with corresponding metrics for the Viterbi decoder. For QPSK, the demapping is simply taking the in-phase and quadrature values as the two desired metrics. For the case of 16-QAM, the in-phase and quadrature values are treated as independent 4 level PAM signals, which are demapped into 2 metrics as shown in Figure 3.9. Here, the input values are normalized such that 2 corresponds to a decision

level, above which $b1$ is zero. The scale of the output values depends on the required quantization level of the Viterbi decoder, which typically ranges from 3 to 8 bits. Notice that the metric for b0 can be twice as large as for b1 in case the in-phase or quadrature value is –3 or +3. This indicates the fact that the b0 values are indeed more reliable in this case, as the minimum Euclidean distance from a +3 value to an erroneous $b0$ value of –1 is 4, while the minimum distance between two different $b1$ values is always 2. This difference in reliability of bits becomes even larger for higher order QAM. For instance, Figure 3.10 shows the demapping of 3-bit metrics for the case of 8 level PAM, which is used to make a 64-QAM constellation.

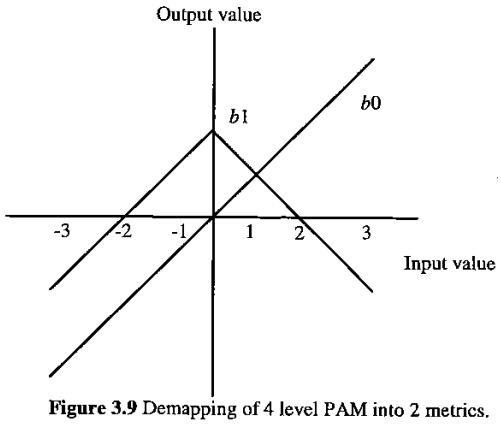

Figure 3.9 Demapping of 4 level PAM into 2 metrics.

Figure 3.11 shows the BERs versus E_b/N_o for several combinations of coding rates and QAM types in an AWGN channel. An interesting effect is that the coding gain relative to the uncoded QAM curves of Figure 3.7 becomes larger for larger QAM constellations. At a BER of 10^{-5}, for instance, the coding gains for a rate 1/2 code are approximately 5.5, 7, and 8.5 dB for QPSK, 16-QAM, and 64-QAM, respectively. This is explained by the fact that the uncoded error probability is determined mainly by the least significant bits in the Gray mapping; for instance, the b3 values in Figure 3.10. When coding is used, then the error probability depends on an average over several coded bits; for instance, several b1, b2, and b3 values in the case of 64-QAM. As a result of this averaging, the minimum squared Euclidean distance between different coded QAM sequences is larger than in the situation where only the least significant bits like b3 in Figure 3.10 are transmitted. Therefore, the coding gain is larger than in the case of QPSK or BPSK, where all bits have the same weight.

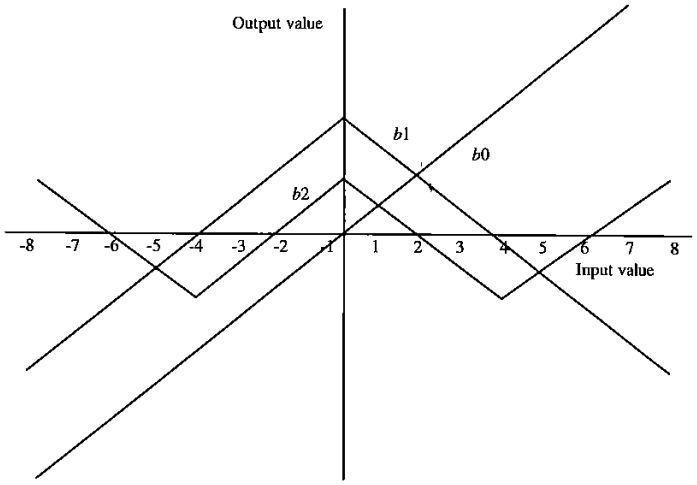

Figure 3.10 Demapping of 8 level PAM into 3 metrics.

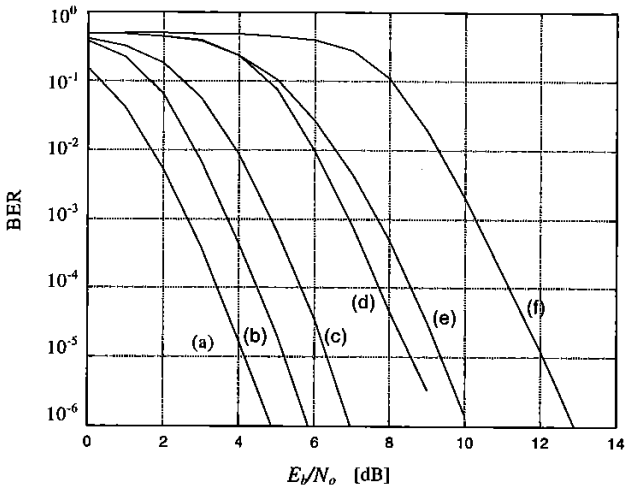

Figure 3.11 BERs versus E_b/N_o in AWGN for a constraint length 7 convolutional code with (a) QPSK, rate ½, (b) QPSK, rate ¾; (c) 16-QAM, rate ½; (d) 16-QAM, rate ¾; (e) 64-QAM, rate ½; (f) 64-QAM, rate ¾.

Other interesting information that can be derived from Figure 3.11 is the coding gain of a particular coded modulation type when compared with the uncoded QAM constellation that gives the same net data rate or the same efficiency in bps/Hz. For instance, the curve for 16-QAM with rate 1/2 coding can be compared with the curve for uncoded QPSK in Figure 3.7, as both have the same efficiency of 2 bps/Hz. It can be seen from the figures that for a BER of 10^{-5}, coded 16-QAM gives a coding gain of about 3 dB, compared with that of uncoded QPSK.

Figure 3.12 shows simulated BERs versus mean E_b/N_o for a Rayleigh fading channel with an exponentially decaying power delay profile. This channel was introduced in Chapter 1. Curves are drawn for various normalized delay spreads $\tau_{rms}N_s/T$, which is the rms delay spread as defined in Chapter 1 multiplied by the bandwidth of the OFDM signal. The normalized delay spread makes it possible to generalize delay spread results, independent of the number of subcarriers or the absolute bandwidth value of an OFDM system. It is required though that the number of subcarriers be significantly larger (a factor of 4 is sufficient) than the constraint length of the convolutional code, such that the code is able to fully benefit from the frequency diversity of the channel. The fact that the performance of an OFDM link depends only on the normalized delay spread $\tau_{rms}N_s/T$ can be understood better by realizing that the rms delay spread is approximately equal to the inverse of the coherence bandwidth of the channel, which determines the characteristics of bandwidth and spacing of fades in the channel frequency response. A small normalized delay spread is equivalent to a small ratio of OFDM signal bandwidth and coherence bandwidth. In such a situation, the channel frequency response is relatively flat within the OFDM signal bandwidth, so if there is a deep fade, all the subcarriers are significantly attenuated. In the case of a large normalized delay spread, a fade only affects a few adjacent subcarriers. There can be several fades within the OFDM signal bandwidth, with relatively strong subcarriers between the fades. As a result, the average signal power is much more constant over several channels than in the case of small delay spreads. The coding benefits from this by using the stronger subcarriers to compensate for the attenuated subcarriers.

Except for the delay spread, the guard time T_G is also normalized in Figure 3.12 and all other figures in this chapter. The normalized guard time is defined here as T_GN_s/T; the same normalization as for the guard time is applied to maintain a fixed ratio between delay spread and guard time, independent of the number of subcarriers N_s and the FFT interval T. Because the E_b/N_o loss caused by the guard time depends on the ratio T_G/T_s rather than the normalization chosen here, the guard time loss is not included in the following figures. This makes it possible to see from Figure 3.12 for what ratio of guard time and delay spread the system breaks down because of ISI and ICI. In Figure 3.12, for instance, an error floor is starting to appear for a normalized delay spread of 4; the ratio of guard time and delay spread is 3 for this case. Hence, for QPSK with rate 3/4 coding, the guard time should be at least three times the delay spread to achieve an average BER less than 10^{-4}.

derived from Figure 3.11 is the coding
en compared with the uncoded QAM
or the same efficiency in bps/Hz. For
oding can be compared with the curve
he same efficiency of 2 bps/Hz. It can
coded 16-QAM gives a coding gain of
K.

ius mean E_b/N_o for a Rayleigh fading
er delay profile. This channel was
or various normalized delay spreads
fined in Chapter 1 multiplied by the
ed delay spread makes it possible to
of the number of subcarriers or the
t is required though that the number of
is sufficient) than the constraint length
ible to fully benefit from the frequency
mance of an OFDM link depends only
understood better by realizing that the
inverse of the coherence bandwidth of
s of bandwidth and spacing of fades in
alized delay spread is equivalent to a
erence bandwidth. In such a situation,
within the OFDM signal bandwidth, so
gnificantly attenuated. In the case of a
is a few adjacent subcarriers. There can
vidth, with relatively strong subcarriers
nal power is much more constant over
spreads. The coding benefits from this
for the attenuated subcarriers.

ne T_G is also normalized in Figure 3.12
nalized guard time is defined here as
time is applied to maintain a fixed ratio
ent of the number of subcarriers N_s and
sed by the guard time depends on the
sen here, the guard time loss is not
t possible to see from Figure 3.12 for
ystem breaks down because of ISI and
is starting to appear for a normalized
lay spread is 3 for this case. Hence, for
ould be at least three times the delay

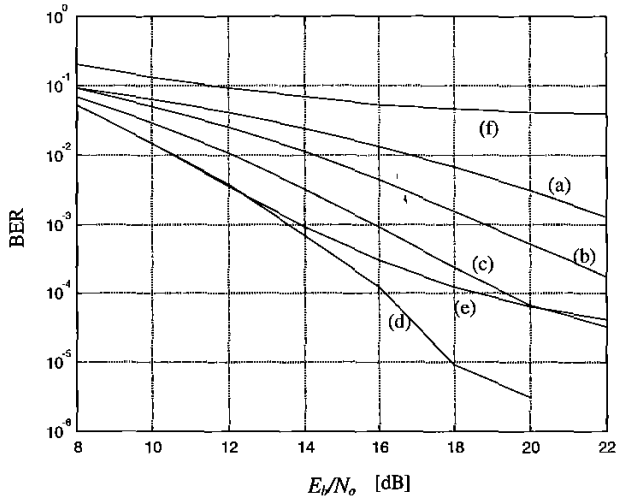

Figure 3.12 BERs versus mean E_b/N_o in a Rayleigh fading channel for QPSK, rate 3/4 convolutional coding, normalized guard time $T_GN_s/T = 12$, normalized delay spread $\tau_{rms}N_s/T$ = (a) 0.25, (b) 0.5, (c) 1, (d) 2, (e) 4, (f) 8.

Notice that Figure 3.12 uses the mean E_b/N_o, which is the average value over a large number of independent channels. The instantaneous E_b/N_o of an individual channel can be significantly smaller or larger than this mean value, especially for low delay spreads where the instantaneous signal power is determined by a single Rayleigh fading path. For larger delay spreads, the variation in the instantaneous signal power becomes much smaller because of the increased frequency diversity of the channel. Low instantaneous E_b/N_o values, which dominate the error ratio, occur much less frequently than at low delay spreads, hence the improved performance. The larger the delay spread, the smaller the E_b/N_o can be, until the delay spread becomes so large that ISI and ICI become limiting factors.

Figure 3.13 shows packet-error ratios (PERs) for 256-byte packets, simulated for the same conditions as Figure 3.12. For relatively slowly time-varying channels, as encountered for instance in indoor wireless LAN applications, the packet-error ratio averaged over a large number of fading channels is equivalent to the coverage outage probability, which is the probability of an unacceptably large packet-error ratio at a certain location within the coverage range. For instance, at an E_b/N_o value of 18 dB and a normalized delay spread between 0.5 and 4, a packet error ratio of 1% means that 1% of the channels generate most of the packet errors—caused by deep fades or ISI/ICI—while the remaining 99% of the channels have a much lower error ratio.

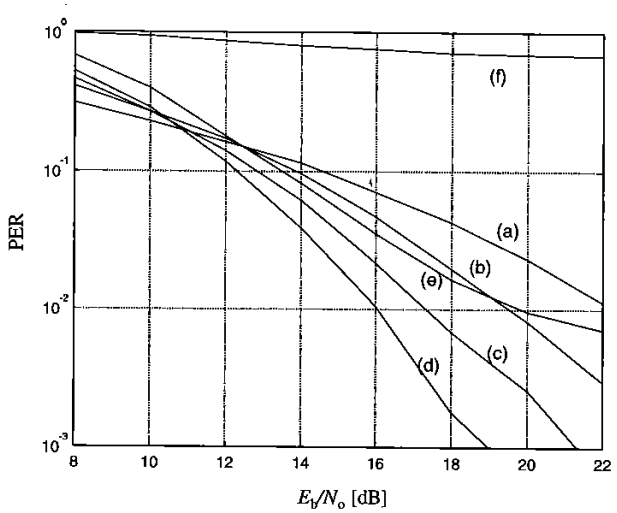

Figure 3.13 PERs versus mean E_b/N_o in a Rayleigh fading channel for QPSK, rate 3/4 convolutional coding, packet length = 256 bytes, normalized guard time $T_G N/T$ = 12, normalized delay spread $\tau_{rms} N_s/T$ = (a) 0.25, (b) 0.5, (c) 1, (d) 2, (e) 4, (f) 8.

Figure 3.14 shows simulated BERs and PERs for 256-byte packets in a Rayleigh fading channel with an exponentially decaying power delay profile. Two different combinations of coding rate and QAM type are used. Curves (a) and (c) are based on 16-QAM with rate 1/2 coding, giving a spectral efficiency of 2 bps/Hz, while curves (b) and (d) use QPSK with rate 3/4 coding, giving an efficiency of 1.5 bps/Hz. This example leads to the surprising result that in a fading channel, a higher order QAM system with a better spectral efficiency can be actually better in terms of E_b/N_o performance than a system with a lower spectral efficiency based on a lower order QAM, while the opposite is true in AWGN as demonstrated by Figure 3.11. The explanation for this effect is that in a frequency selective channel where a certain percentage of the subcarriers can be completely lost in deep fades, the ability to correct for those lost subcarriers by having a large Hamming distance is more important than a large minimum Euclidean distance for each individual subcarrier. In the example of Figure 3.11, the rate 1/2 code combined with 16-QAM can tolerate more weak subcarriers than the rate 3/4 code with QPSK, resulting in an E_b/N_o gain that is larger than the loss in Euclidean distance of 16-QAM versus QPSK.

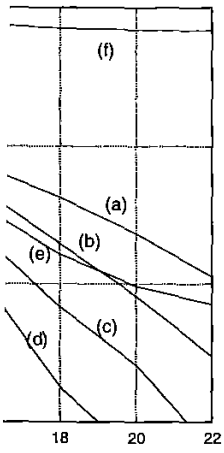

ng channel for QPSK, rate 3/4 convolutional
:d guard time $T_G N/T = 12$, normalized delay
(e) 4, (f) 8.

nd PERs for 256-byte packets in a
/ decaying power delay profile. Two
type are used. Curves (a) and (c) are
ı spectral efficiency of 2 bps/Hz, while
ng, giving an efficiency of 1.5 bps/Hz.
it in a fading channel, a higher order
an be actually better in terms of E_b/N_o
ral efficiency based on a lower order
as demonstrated by Figure 3.11. The
ıcy selective channel where a certain
lost in deep fades, the ability to correct
ming distance is more important than a
lividual subcarrier. In the example of
h 16-QAM can tolerate more weak
esulting in an E_b/N_o gain that is larger
ersus QPSK.

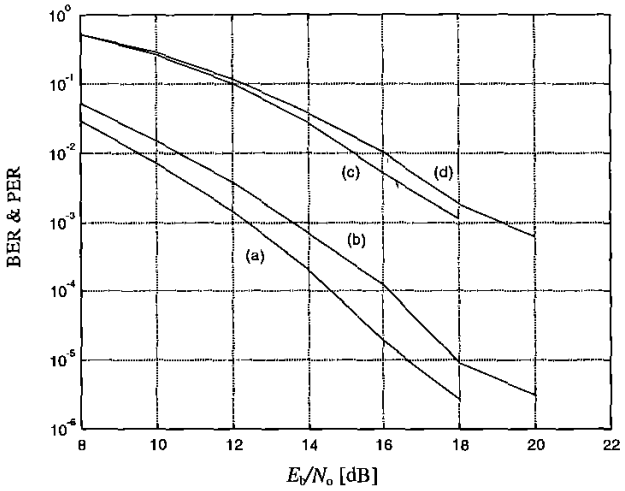

Figure 3.14 PER and BER versus mean E_b/N_o in a Rayleigh fading channel for a packet length of 256 bytes and a normalized delay spread $\tau_{rms}N_s/T = 2$. (a) BER of 16-QAM, rate 1/2 coding; (b) BER of QPSK, rate 3/4 coding; (c) PER of 16-QAM, rate 1/2 coding; (d) PER of QPSK, rate 3/4 coding.

As mentioned before, when the delay spread increases, the performance of an OFDM link increases until a limit is reached where ISI and ICI cause an unacceptably high error floor. This error floor depends on the type of modulation and coding rate. Figure 3.15 illustrates this with simulation curves of the packet error floor versus the normalized delay spread τ_{rms}/T_G. No noise was present in the simulations, so all errors are purely caused by ISI and ICI. As expected, more delay spread can be tolerated for smaller QAM constellations. There is little difference, however, in the robustness of, for instance QPSK with rate 3/4 coding and 16-QAM with rate 1/2 coding, thanks to the fact that the latter is able to tolerate more erroneous subcarriers, which partly compensates the smaller distance between constellation points.

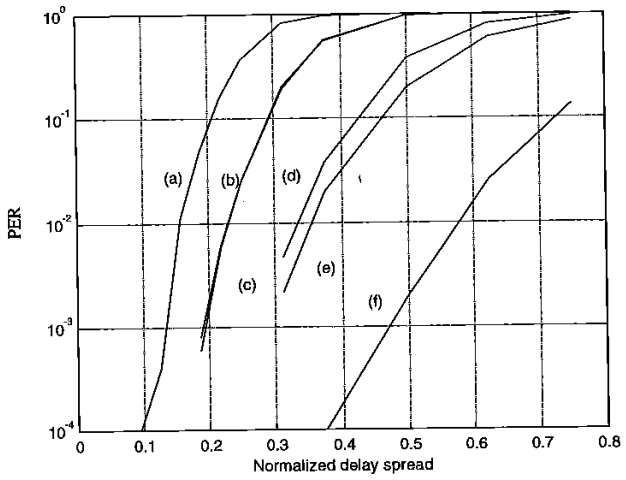

Figure 3.15 Irreducible packet error ratios versus normalized delay spread τ_{rms}/T_G for 256 byte packets and (a) 64-QAM, rate ¾; (b) 64-QAM, rate ½; (c) 16-QAM, rate ¾; (d) 16-QAM, rate ½; (e) QPSK, rate ¾; (f) QPSK, rate ½.

When an OFDM system has to be designed, Figure 3.15 can be used to derive a minimum requirement on the guard time, based on the maximum delay spread for which the system should work. For instance, for a tolerable packet-error floor of 1%, the guard time has to be about twice the delay spread for QPSK with rate 1/2 coding, but it has to be six times the delay spread for 64-QAM with rate 3/4 coding.

REFERENCES

[1] Wesel, R. D., "Joint Interleaver and Trellis Code Design," *Proceedings of IEEE Globecom*, 1997.

[2] Le Floch, B., M. Alard, and C. Berrou, "Coded Orthogonal Frequency Division Multiplex," *Proceedings of the IEEE*, Vol. 83, no. 6, June 1995.

[3] Alard, M., and R. Lasalle, "Principles of Modulation and Channel Coding for Digital Broadcasting for Mobile Receivers," *EBU Technical Review*, No. 224, pp. 168 - 190.

[4] Wang, Q., and L. Y. Onotera, "Coded QAM Using a Binary Convolutional Code," *IEEE Transactions on Communications*, Vol. 43, No. 6, June 1995.

[5] Wesel, R. D., and J. M. Cioffi, "Fundamentals of Coding for Broadcast OFDM," *Proceedings of IEEE ASILOMAR-29*, 1996.

[6] Massey, J. L., "Shift-Register Synthesis and BCH Decoding," *IEEE Transactions on Information Theory*, IT-15, pp. 122 - 127, Jan. 1979.

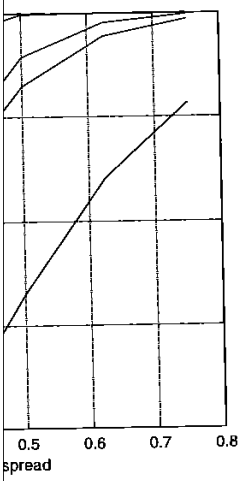

zed delay spread τ_{rms}/T_G for 256 byte packets (c) 16-QAM, rate ¾; (d) 16-QAM, rate ½; (e)

ed, Figure 3.15 can be used to derive a d on the maximum delay spread for r a tolerable packet-error floor of 1%, spread for QPSK with rate 1/2 coding, QAM with rate 3/4 coding.

s Code Design," *Proceedings of IEEE*

Coded Orthogonal Frequency Division 83, no. 6, June 1995.

f Modulation and Channel Coding for ," *EBU Technical Review*, No. 224, pp.

QAM Using a Binary Convolutional *tions*, Vol. 43, No. 6, June 1995.

ntals of Coding for Broadcast OFDM," 6.

nd BCH Decoding," *IEEE Transactions* 27, Jan. 1979.

[7] Berlekamp, E. R., "The Technology of Error Correcting Codes," *Proceedings of the IEEE*, Vol.68, No.5, pp.564 – 593, May 1980.

[8] Charles Lee, L. H., "*Convolutional Coding: Fundamentals and Applications*," London: Artech House, 1997.

[9] Ungerboeck, G., "Channel Coding with Multilevel/Phase Signals," *IEEE Transactions on Information Theory*, Vol. IT-28, No.1, pp.55-67, Jan. 1982.

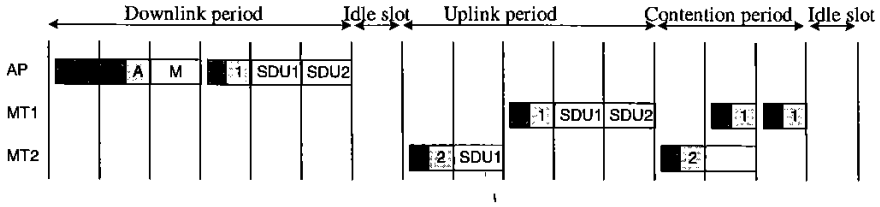

Figure 10.9 Magic WAND MAC frame.

The master scheduler, which must be able to schedule the transmissions of any mix of ATM traffic classes, employs a leaky-bucket-based scheme where the highest priority is given to constant bit-rate traffic, the second priority to variable bit rate, and so on. Tokens, which are generated at a constant rate, fill a bucket. The scheduler takes tokens from the bucket, and translates them in the allocation of slots in the slot map according to the connections' delay requirements. A traffic source can request slots (access points directly, mobile terminals use piggy-backed and contention requests) in excess of the mean rate. Depending on the negotiated burstiness of the source, which is reflected in a commensurate bucket depth, the scheduler grants the request. Effectively, the scheduler polices and shapes the traffic on the wireless link, to guarantee delay QoS compliance for all connections. See [7] for an extensive discussion of scheduling.

The second important measure of QoS, besides delay and delay jitter, is the connection's error performance over the wireless ATM link. In WAND, the radio physical layer provides a constant service that can meet typical real-time service requirements (e.g., for a voice service). TCP/IP-based data connections cannot tolerate high cell loss ($> 10^{-2}$) and these are protected by ARQ. Third, there are services such as video requiring real-time service with low error probability. The solution applied in WAND is to apply ARQ with a limited number of retransmissions.

10.5 IEEE 802.11, HIPERLAN/2 AND MMAC WIRELESS LAN STANDARDS

Since the beginning of the nineties, wireless local area networks (WLAN) for the 900-MHz, 2.4-GHz, and 5-GHz ISM (Industrial, Scientific, & Medical) bands have been available, based on a range of proprietary techniques. In June 1997, the Institute of Electrical and Electronics Engineers (IEEE) approved an international interoperability standard [8]. The standard specifies both medium access control (MAC) procedures and three different physical layers (PHY). There are two radio-based PHYs using the 2.4-GHz band. The third PHY uses infrared light. All PHYs support a data rate of 1 Mbps and optionally 2 Mbps. The 2.4-GHz frequency band is available for license-exempt use in Europe, the United States, and Japan. Table 10.3

lists the available frequency band and the restrictions to devices which use this band for communications.

Table 10.3
International 2.4-GHz ISM bands.

Location	Regulatory range	Maximum output power
North America	2.400–2.4835 GHz	1,000 mW
Europe	2.400–2.4835 GHz	100 mW (EIRP*)
Japan	2.471–2.497 GHz	10 mW

* EIRP = effective isotropic radiated power.

User demand for higher bit rates and the international availability of the 2.4-GHz band has spurred the development of a higher speed extension to the 802.11 standard. In July 1998, a proposal was selected for standardization, which describes a PHY providing a basic rate of 11 Mbps and a fall back rate of 5.5 Mbps. This PHY can be seen as a fourth option, to be used in conjunction with the MAC that is already standardized. Practical products, however, are expected to support both the high-speed 11- and 5.5-Mbit/s rates mode as well as the 1- and 2-Mbps modes.

A second IEEE 802.11 working group has moved on to standardize yet another PHY option, which offers higher bit rates in the 5.2-GHz band. This development was motivated by the adoption, in January 1997, by the U.S. Federal Communications Commission, of an amendment to Part 15 of its rules. The amendment makes available 300 MHz of spectrum in the 5.2-GHz band, intended for use by a new category of unlicensed equipment called Unlicensed National Information Infrastructure (UNII) devices [9]. Table 10.4 lists the frequency bands and the corresponding power restrictions. Notice that the maximum permitted output power depends on the emission bandwidth; for a bandwidth of 20 MHz, you are allowed to transmit at the maximum power levels listed in the middle column of Table 10.4. For a bandwidth smaller than 20 MHz the power limit reduces to the value specified in the right column.

Table 10.4
United States 5.2 GHz U-NII band.

Location	Maximum output power minimum of	
5.150–5.250 GHz	50 mW	4 dBm + $10\log_{10}$B*
5.250–5.350 GHz	250 mW	11 dBm + $10\log_{10}$ B
5.725–5.825 GHz	1,000 mW	17 dBm + $10\log_{10}$ B

* B is the –26-dB emission bandwidth in MHz.

Like the IEEE 802.11 standard, the European ETSI HIPERLAN type 1 standard [10] specifies both MAC and PHY. Unlike IEEE 802.11, however, no HIPERLAN type 1 compliant products are available in the market place. A newly formed ETSI working group called Broadband Radio Access Networks (BRAN) is now working on

ons to devices which use this band for

SM bands.

e	Maximum output power
z	1,000 mW
z	100 mW (EIRP*)
	10 mW

adiated power.

international availability of the 2.4- igher speed extension to the 802.11 or standardization, which describes a back rate of 5.5 Mbps. This PHY can nction with the MAC that is already pected to support both the high-speed d 2-Mbps modes.

moved on to standardize yet another 5.2-GHz band. This development was y the U.S. Federal Communications ules. The amendment makes available ended for use by a new category of al Information Infrastructure (UNII) ands and the corresponding power utput power depends on the emission allowed to transmit at the maximum e 10.4. For a bandwidth smaller than ified in the right column.

-NII band.

Maximum output power minimum of	
0 mW	4 dBm + $10\log_{10}B$*
50 mW	11 dBm + $10\log_{10}B$
00 mW	17 dBm + $10\log_{10}B$

dwidth in MHz.

an ETSI HIPERLAN type 1 standard 802.11, however, no HIPERLAN type place. A newly formed ETSI working orks (BRAN) is now working on extensions to the HIPERLAN standard. Three extensions are under development: HIPERLAN/2, a wireless indoor LAN with a QoS provision; HiperLink, a wireless indoor backbone; and HiperAccess, an outdoor, fixed wireless network providing access to a wired infrastructure.

In Japan, equipment manufacturers, service providers and the Ministry of Post and Telecommunications are cooperating in the Multimedia Mobile Access Communication (MMAC) project to define new wireless standards similar to those of IEEE 802.11 and ETSI BRAN. Additionally, MMAC is also looking into the possibility for ultra-high-speed wireless indoor LANs supporting large-volume data transmission at speeds up to 156 Mbps using frequencies in the 30– to 300– GHz band.

In July 1998, the IEEE 802.11 standardization group decided to select OFDM as the basis for their new 5-GHz standard, targeting a range of data rates from 6 up to 54 Mbps [12, 13]. This new standard is the first one to use OFDM in packet-based communications, while the use of OFDM until now was limited to continuous transmission systems like DAB and DVB. Following the IEEE 802.11 decision, ETSI BRAN and MMAC also adopted OFDM for their physical layer standards. The three bodies have worked in close cooperation since then to make sure that differences among the various standards are kept to a minimum, thereby enabling the manufacturing of equipment that can be used worldwide.

The focus of this section is on the physical layer side. In the case of the IEEE 802.11 standard, the MAC layer for the higher data rates remains the same as for the currently supported 1- and 2- Mbps rates. A description of this MAC can be found in [11].

10.5.1 OFDM Parameters

Table 10.5 lists the main parameters of the draft OFDM standard. A key parameter that largely determined the choice of the other parameters is the guard interval of 800 ns. This guard interval provides robustness to rms delay spreads up to several hundreds of nanoseconds, depending on the coding rate and modulation used. In practice, this means that the modulation is robust enough to be used in any indoor environment, including large factory buildings. It can also be used in outdoor environments, although directional antennas may be needed in this case to reduce the delay spread to an acceptable amount and increase the range.

Table 10.5
Main parameters of the OFDM standard.

Data rate	6, 9, 12, 18, 24, 36, 48, 54 Mbps
Modulation	BPSK, QPSK, 16-QAM, 64-QAM
Coding rate	1/2, 2/3, 3/4
Number of subcarriers	52
Number of pilots	4
OFDM symbol duration	4 μs
Guard interval	800 ns
Subcarrier spacing	312.5 kHz
–3-dB Bandwidth	16.56 MHz
Channel spacing	20 MHz

To limit the relative amount of power and time spent on the guard time to 1 dB, the symbol duration chosen is 4 μs. This also determines the subcarrier spacing at 312.5 kHz, which is the inverse of the symbol duration minus the guard time. By using 48 data subcarriers, uncoded data rates of 12 to 72 Mbps can be achieved by using variable modulation types from BPSK to 64-QAM. In addition to the 48 data subcarriers, each OFDM symbol contains an additional four pilot subcarriers, which can be used to track the residual carrier frequency offset that remains after an initial frequency correction during the training phase of the packet.

To correct for subcarriers in deep fades, forward-error correction across the subcarriers is used with variable coding rates, giving coded data rates from 6 up to 54 Mbps. Convolutional coding is used with the industry standard rate 1/2, constraint length 7 code with generator polynomials (133,171). Higher coding rates of 2/3 and 3/4 are obtained by puncturing the rate 1/2 code. The 2/3-rate is used together with 64-QAM only to obtain a data rate of 48 Mbps. The 1/2-rate is used with BPSK, QPSK, and 16-QAM to give rates of 6, 12, and 24 Mbps, respectively. Finally, the 3/4-rate is used with BPSK, QPSK, 16-QAM, and 64-QAM to give rates of 9, 18, 36, and 54 Mbps, respectively.

10.5.2 Channelization

Figure 10.10 shows the channelization for the lower and middle UNII bands. Eight channels are available with a channel spacing of 20 MHz and guard spacings of 30 MHz at the band edges in order to meet the stringent FCC-restricted band spectral density requirements. The FCC also defined an upper UNII band from 5.725 to 5.825 GHz, which carries another four OFDM channels. For this upper band, the guard spacing from the band edges is only 20 MHz, as the out-of-band spectral requirements for the upper band are less severe than those of the lower and middle UNII bands. In Europe, a total of 455 MHz is available in two bands, one from 5.15 to 5.35 GHz and

FDM standard.

, 9, 12, 18, 24, 36, 48, 54 Mbps
BPSK, QPSK, 6-QAM, 64-QAM
1/2, 2/3, 3/4
52
4
4 µs
800 ns
312.5 kHz
16.56 MHz
20 MHz

d time spent on the guard time to 1 dB, ermines the subcarrier spacing at 312.5 on minus the guard time. By using 48 Mbps can be achieved by using variable ddition to the 48 data subcarriers, each subcarriers, which can be used to track ns after an initial frequency correction

s, forward-error correction across the iving coded data rates from 6 up to 54 industry standard rate 1/2, constraint 71). Higher coding rates of 2/3 and 3/4 The 2/3-rate is used together with 64- he 1/2-rate is used with BPSK, QPSK, ps, respectively. Finally, the 3/4-rate is AM to give rates of 9, 18, 36, and 54

lower and middle UNII bands. Eight of 20 MHz and guard spacings of 30 stringent FCC-restricted band spectral upper UNII band from 5.725 to 5.825 nels. For this upper band, the guard s the out-of-band spectral requirements f the lower and middle UNII bands. In bands, one from 5.15 to 5.35 GHz and

another from 5.470 to 5.725 GHz. In Japan, a 100 MHz wide band is available from 5.15 to 5.25 GHz, carrying four OFDM channels.

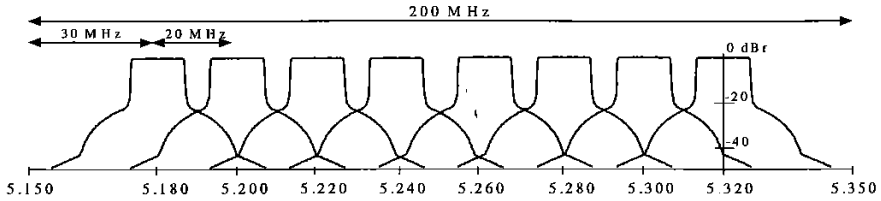

Figure 10.10 Channelization in lower and middle UNII band.

10.5.3 OFDM Signal Processing

The general block diagram of the baseband processing of an OFDM transceiver is shown in Figure 10.11. In the transmitter path, binary input data is encoded by a standard rate 1/2 convolutional encoder. The rate may be increased to 2/3 or 3/4 by puncturing the coded output bits. After interleaving, the binary values are converted into QAM values. To facilitate coherent reception, four pilot values are added to each 48 data values, so a total of 52-QAM values is reached per OFDM symbol, which are modulated onto 52 subcarriers by applying the IFFT. To make the system robust to multipath propagation, a cyclic prefix is added. Further, windowing is applied to attain a narrower output spectrum. After this step, the digital output signals can be converted to analog signals, which are then up-converted to the 5-GHz band, amplified and transmitted through an antenna.

The OFDM receiver basically performs the reverse operations of the transmitter, together with additional training tasks. First, the receiver has to estimate frequency offset and symbol timing, using special training symbols in the preamble. Then, it can do an FFT for every symbol to recover the 52-QAM values of all subcarriers. The training symbols and pilot subcarriers are used to correct for the channel response as well as remaining phase drift. The QAM values are then demapped into binary values, after which a Viterbi decoder can decode the information bits.

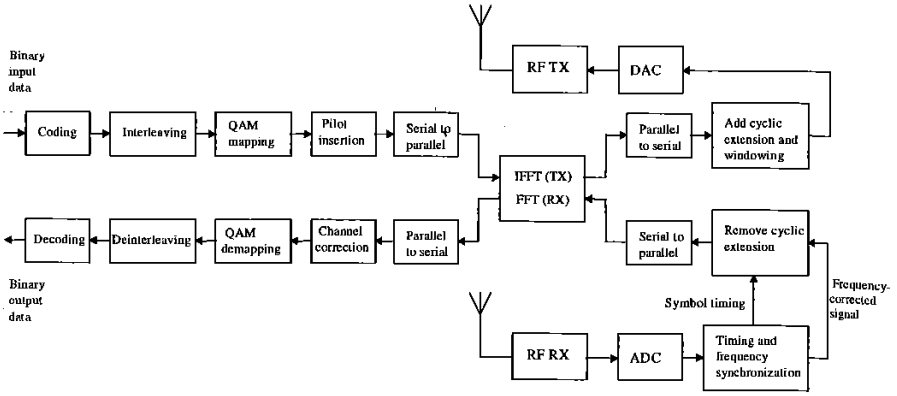

Figure 10.11 Block diagram of OFDM transceiver.

10.5.4 Training

Figure 10.12 shows the structure of the preamble that preceeds every OFDM packet. This preamble is essential to perform start-of-packet detection, automatic gain control, symbol timing, frequency estimation, and channel estimation. All of these training tasks have to be performed before the actual data bits can be successfully decoded.

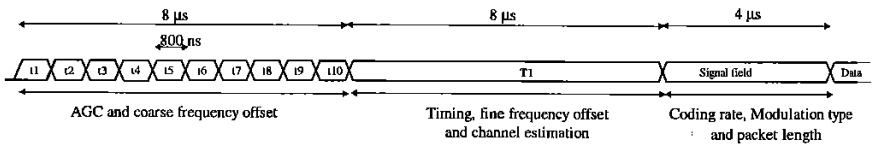

Figure 10.12 OFDM preamble.

The first part of the preamble consists of 10 repetitions of a training symbol with a duration of 800 ns each, which is only a quarter of the FFT duration of a normal data symbol. These short symbols are produced by using only nonzero subcarrier values for subcarrier numbers that are a multiple of 4. Hence, of all possible subcarrier numbers from –26 to +26, only the subset {–24, –20, –16, –12, –8, –4, 4, 8, 12, 16, 20, 24} is used. There are two reasons for using relatively short symbols in this part of the training; first, the short symbol period makes it possible to do a coarse frequency offset estimation with a large unambiguous range. For a repetitive signal with a duration of T, the maximum measurable unambiguous frequency offset is equal to $1/(2T)$, as higher frequency offsets result in a phase change exceeding π from one symbol to another. Hence, by measuring the phase drift between two consecutive short symbols with a

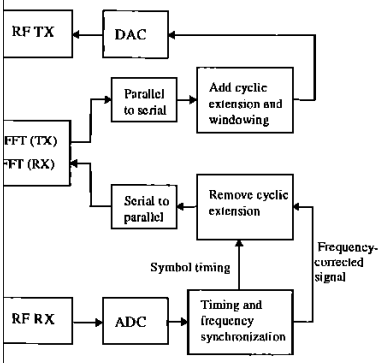

)M transceiver.

hat preceeds every OFDM packet. t detection, automatic gain control, timation. All of these training tasks be successfully decoded.

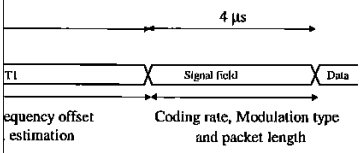

mble.

0 repetitions of a training symbol ter of the FFT duration of a normal by using only nonzero subcarrier 4. Hence, of all possible subcarrier), –16, –12, –8, –4, 4, 8, 12, 16, 20, ly short symbols in this part of the ible to do a coarse frequency offset petitive signal with a duration of T, offset is equal to $1/(2T)$, as higher ng π from one symbol to another. consecutive short symbols with a

duration of 800 ns, frequency offsets up to 625 kHz can be estimated. If training symbols with a duration equal to the FFT interval of 3.2 µs were used, then the maximum frequency offset of only 156 kHz could be measured, corresponding to a relative frequency error of about 26 ppm at a carrier frequency of 5.8 GHz. The IEEE 802.11 standard specifies a maximum offset *per user* of 20 ppm, which means that the worst case offset as seen by a receiver can be up to 40 ppm, as it experiences the sum of the frequency offsets from both transmitter and receiver.

The second reason for using short symbols at the start of the training is that they provide a convenient way of performing AGC and frame detection. Detection of the presence of a packet can be done by correlating a short symbol with the next and detecting if the correlation magnitude exceeds some threshold. After each interval equal to two short symbol durations, the receiver gain can be adjusted after which detection and gain measuring can continue. Of course, this AGC algorithm could also be applied to long training symbols, but the advantage of short symbols is that we have more repetitions in the same amount of time, which makes it easier to do several measurements and gain adjustments during the training.

The short training symbols are followed by a long training symbol (T1) that contains 52 QPSK-modulated subcarriers like a normal data symbol. The length of this training symbol is twice that of a data symbol, however, which is done for two reasons. First, it makes it possible to do a precise frequency estimation on the long symbol. The long symbol is formed by cyclically extending the IFFT output signal to a length of 8 µs. Thus, it contains two and a half times the original IFFT duration. The first 1.6 µs serves as a guard interval, containing a copy of the last 1.6 µs of the IFFT output. The long training symbol makes it possible to do a fine frequency offset estimation by measuring the phase drift between samples that are 3.2 µs apart within the long training symbol. The second reason for having the long symbol is to obtain reference amplitudes and phases for doing coherent demodulation. By averaging the two identical parts of the long training symbol, coherent references can be obtained with a noise level that is 3 dB lower than the noise level of data symbols.

Both the long and short symbols are designed in such a way that the PAP ratio is approximately 3 dB, which is significantly lower than the PAP ratio of random OFDM data symbols. This guarantees the training degradation caused by nonlinear amplifier distortion to be smaller than the distortion of the data symbols. It also allows the use of a simple correlator implementation at the receiver as explained in Section 4.6.

After the preamble, there is still one training task left, which is tracking the reference phase. There will always be some remaining frequency offset that causes a common phase drift on all subcarriers. To track this phase drift, 4 of the 52 subcarriers contain known pilot values. The pilots are scrambled by a length 127 pseudonoise sequence to avoid spectral lines exceeding the average power density of the OFDM spectrum.

Figure 10.13 shows the time-fequency structure of an OFDM packet, where all known training values are marked in gray. It clearly illustrates how the packet starts with 10 short training symbols, using only 12 subcarriers, followed by the long training symbol and data symbols, with each data symbol containing four known pilot subcarriers.

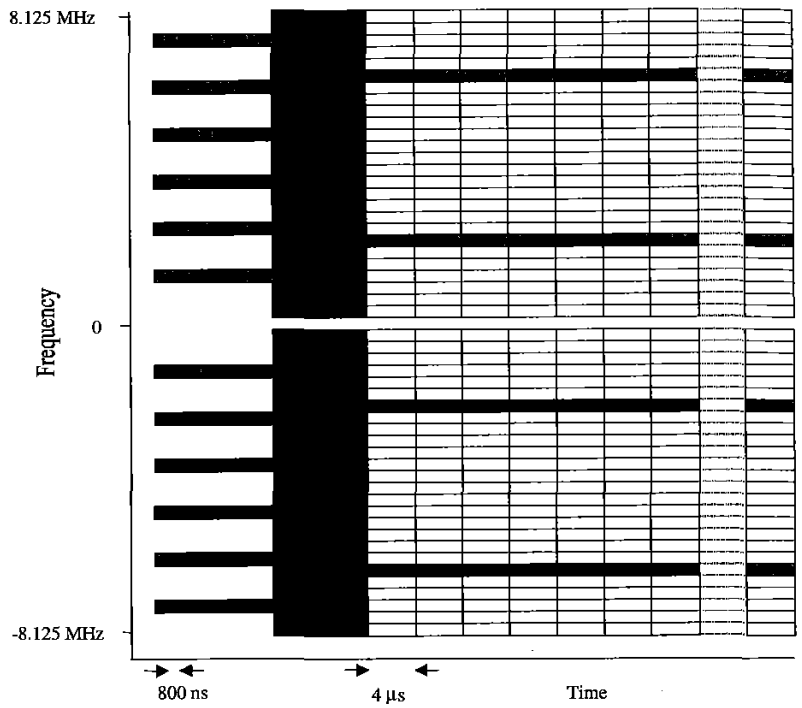

Figure 10.13 Time-frequency structure of an OFDM packet. Gray subcarriers contain known training values.

In the case of the IEEE 802.11 standard, at the end of the preamble a special OFDM data symbol at the lowest 6-Mbps rate is sent, which contains information about the length, modulation type, and coding rate of the rest of the packet. Sending this information at the lowest possible rate ensures that the dynamic rate selection is at least as reliable as the most reliable data rate of 6 Mbps. Further, it makes it possible for all users to decode the duration of a certain packet, even though they may not be able to decode the data content. This is important for the IEEE 802.11 MAC protocol, which specifies that a user has to wait until the end of any packet already in the air before trying to compete for the channel.

tructure of an OFDM packet, where all
learly illustrates how the packet starts
bcarriers, followed by the long training
symbol containing four known pilot

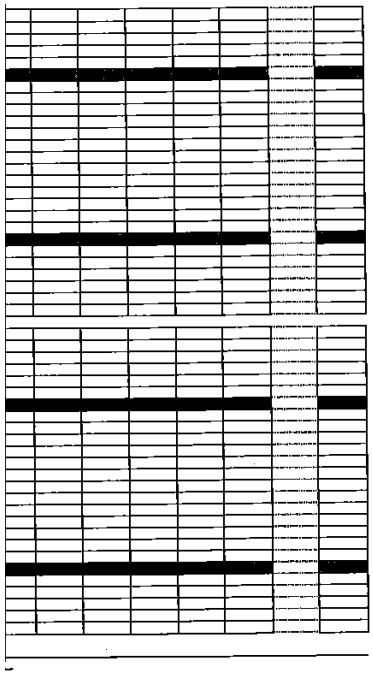

Time

acket. Gray subcarriers contain known training

d, at the end of the preamble a special
s sent, which contains information about
of the rest of the packet. Sending this
hat the dynamic rate selection is at least
bps. Further, it makes it possible for all
t, even though they may not be able to
the IEEE 802.11 MAC protocol, which
of any packet already in the air before

10.5.5 Differences Between IEEE 802.11, HIPERLAN/2 and MMAC

The main differences between IEEE 802.11 and HIPERLAN/2—which is standardized by ETSI BRAN [14]—are in the Medium Access Control (MAC). IEEE 802.11 uses a distributed MAC based on Carrier Sense Multiple Access with Collision Avoidance, (CSMA/CA), while HIPERLAN/2 uses a centralized and scheduled MAC, based on wireless ATM. MMAC supports both of these MACs. As far as the physical layer is concerned, there are a few relatively minor differences between IEEE 802.11 and HIPERLAN/2 which are summarized below:

- HIPERLAN uses different training sequences. The long training symbol is the same as for IEEE 802.11, but the preceding sequence of short training symbols is different. A downlink transmission starts with 10 short symbols as IEEE 802.11, but the first 5 symbols are different in order to detect the start of the downlink frame. The rest of the packets in the downlink frame do not use short symbols, only the long training symbol. Uplink packets may use 5 or 10 identical short symbols, with the last short symbol being inverted.
- HIPERLAN uses extra puncturing to accommodate the tail bits to keep an integer number of OFDM symbols in 54 byte packets. This extra puncturing operation punctures 12 bits out of the first 156 bits of a packet.
- In the case of 16-QAM, HIPERLAN uses a coding rate of 9/16 instead of 1/2—giving a bit rate of 27 instead of 24 Mbps—to get an integer number of OFDM symbols for packets of 54 bytes. The rate 9/16 is made by puncturing 2 out of every 18 encoded bits.
- Both IEEE 802.11 and HIPERLAN scramble the input data with a length 127 pseudo random sequence, but the initialization is different. IEEE 802.11 initializes with 7 random bits which are inserted as the first 7 bits of each packet. In HIPERLAN, the scrambler is initialized by {1, 1, 1} plus the first 4 bits of the Broadcast Channel at the beginning of a MAC frame. The initialization is identical for all packets in a MAC frame.
- HIPERLAN devices have to support power control in the range of -15 to 30 dBm with a step size of 3 dB.
- Dynamic frequency selection is mandatory in Europe over a range of at least 330 MHz for indoor products and 255 MHz (upper band only) for outdoor products. This means that indoor products have to support a frequency range from 5.15 to at least 5.6 GHz, covering the entire lower band and a part of the European upper band. Dynamic frequency selection was included to avoid the need for frequency planning and to provide coexistence with radar systems that operate in the upper part of the European 5 GHz band.

10.5.6 Simulation Results

Figure 10.14 shows the irreducible PER versus delay spread for a few different data rates. This is the minimum possible PER for a certain delay spread, for which all packet errors are caused by intersymbol interference because of path delays exceeding the guard time of the OFDM symbols. Hence, Figure 10.14 demonstrates the delay spread robustness for several data rates. For a 1% PER, the tolerable delay spread is close to 200 ns at 36 Mbps, while at 12 Mbps a delay spread of 450 ns can be tolerated. In practice, this means that the 36-Mbps rate can be used in most indoor environments, except some large factory buildings. The 54 Mbps rate can tolerate delay spreads up to about 120 ns, which is sufficient for most office buildings. The 12-Mbps rate can work in any indoor and even in outdoor environments. This is also true for the lowest rate of 6 Mbps, that is not included in Figure 10.14.

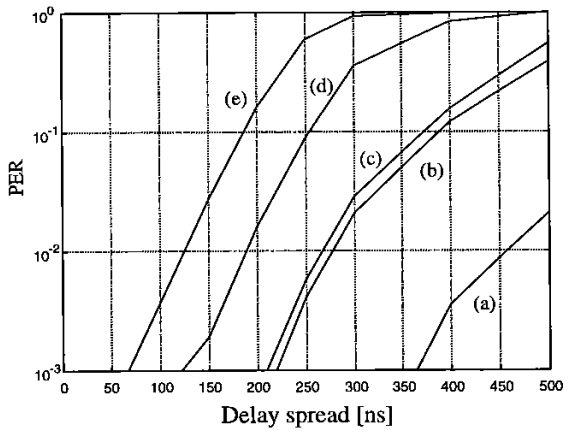

Figure 10.14 PER versus rms delay spread (no noise) for Rayleigh fading paths with an exponentially decaying power delay profile. Packet size is 64 bytes with data rates of (a) 12, (b) 18, (c) 24, (d) 36, and (e) 54 Mbps.

Figure 10.15 shows the PER versus E_b/N_o for a data rate of 24 Mbps in case of an AWGN channel and a Rayleigh fading channel with a delay spread of 100 ns. An E_b/N_o of about 18 dB is required to achieve a 1% PER in the fading channel, which is approximately 6 dB more than what is needed for an ideal Gaussian noise channel. Of course, other data rates have different requirements. Figure 10.16 shows the PER for various data rates as a function of the input power. We can see a difference of almost 18 dB in the signal power requirements of the lowest and highest data rates. This illustrates the importance of fallback rates; users who cannot use the highest rate because they are too far away or are in a bad multipath situation can at least obtain a data link at a lower rate.

delay spread for a few different data
rtain delay spread, for which all packet
ɔecause of path delays exceeding the
e 10.14 demonstrates the delay spread
, the tolerable delay spread is close to
spread of 450 ns can be tolerated. In
ɔe used in most indoor environments,
ɔs rate can tolerate delay spreads up to
buildings. The 12-Mbps rate can work
This is also true for the lowest rate of

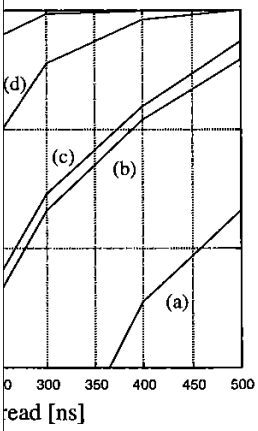

r Rayleigh fading paths with an exponentially
is 64 bytes with data rates of (a) 12, (b) 18,

$_o$ for a data rate of 24 Mbps in case of
nel with a delay spread of 100 ns. An
% PER in the fading channel, which is
or an ideal Gaussian noise channel. Of
ents. Figure 10.16 shows the PER for
r. We can see a difference of almost 18
lowest and highest data rates. This
sers who cannot use the highest rate
ıultipath situation can at least obtain a

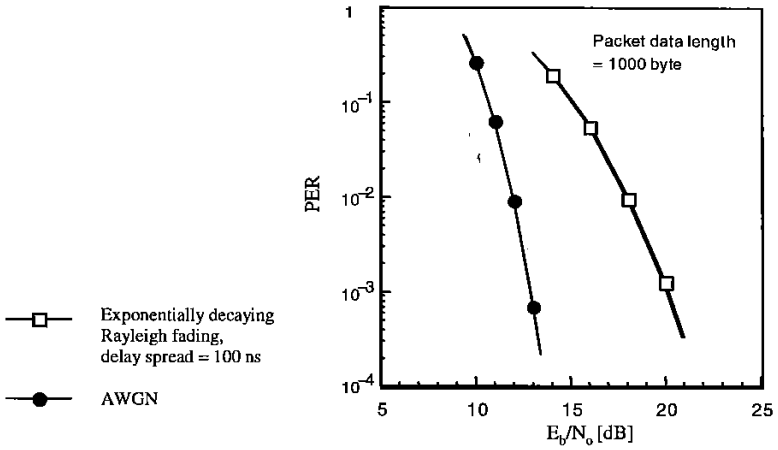

Figure 10.15 PER versus mean E_b/N_o for AWGN and Rayleigh fading with a 100-ns delay spread and a bit rate of 24 Mbps.

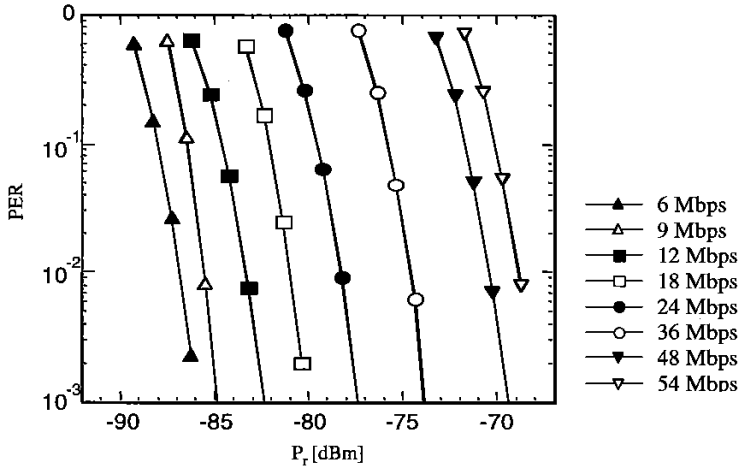

Figure 10.16 PER versus received power level for AWGN and various bit rates.

Figure 10.17 shows simulated spectra of an OFDM signal that is distorted by a nonlinear power amplifier with different backoff values. This is an important subject, because the susceptibility to nonlinear distortion and the need for large backoff values is often mentioned as a disadvantage of OFDM. As shown in [15], however, the effects of nonlinear distortion on the BER are negligible for backoff values of 6 dB or more, where the backoff is defined as the difference between the maximum (saturation) output power and the average output power in dB. The effects on the transmitted spectrum are illustrated in Figure 10.17. We can see that for a 7-dB backoff, the spectrum falls down very steeply after about 8 MHz, and only around 25 dB below the in-band density the spectrum starts to deviate significantly from an ideal undistorted OFDM signal. When the backoff is decreased to 5 dB, the out-of-band spectrum quickly grows toward the outer spectrum mask defined by IEEE 802.11.

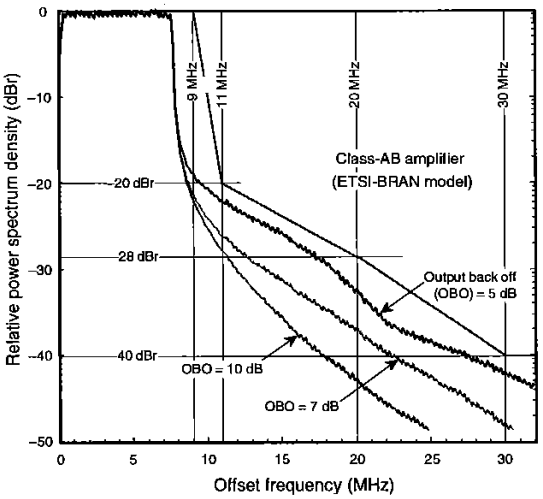

Figure 10.17 OFDM spectrum after a nonlinear power amplifier.

REFERENCES

[1] ETSI, "Radio Broadcasting Systems: Digital Audio Broadcasting to Mobile, Portable and Fixed Receivers," European Telecommunication Standard, ETS 300-401, Feb. 1995.

[2] Tuttlebee, W. H. W., and D. A. Hawkins, "Consumer Digital Radio: From Concept to Reality," *Electronics and Communication Engineering Journal*, Vol. 10, No. 6, pp. 263–276, Dec. 1998.

an OFDM signal that is distorted by a
f values. This is an important subject,
and the need for large backoff values
As shown in [15], however, the effects
e for backoff values of 6 dB or more,
between the maximum (saturation)
dB. The effects on the transmitted
an see that for a 7-dB backoff, the
Hz, and only around 25 dB below the
ignificantly from an ideal undistorted
to 5 dB, the out-of-band spectrum
fined by IEEE 802.11.

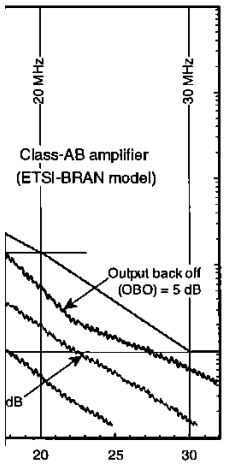

nonlinear power amplifier.

gital Audio Broadcasting to Mobile,
Telecommunication Standard, ETS

ns, "Consumer Digital Radio: From
munication Engineering Journal, Vol.

[3] ETSI, "Digital Video Broadcasting: Framing Structure, Channel Coding, and Modulation for Digital Terrestrial Television," European Telecommunication Standard, EN 300–744, Aug. 1997.

[4] Reimers, U., "DVB-T: The COFDM-Based System for Terrestrial Television," *Electronics and Communication Engineering Journal*, Vol. 9, No. 1, pp. 28–32, Feb. 1997.

[5] Mikkonen, J., J. P. Aldis, G. A. Awater, A. Lunn, and D. Hutchinson, "The Magic WAND—Functional Overview," *IEEE JSAC*, Vol. 16, No. 6, pp. 953–972, Aug. 1998.

[6] Awater, G. A., and J. Ala-Laurila, "Wireless ATM Network Demonstrator," Presentation and Demonstration, *Demo '98 conference*, Berlin, Germany, Oct. 15, 1998.

[7] Passas, N., S. Paskalis, D. Vali, L. Merakis, "Quality-of-Service-Oriented Medium Access Control for Wireless ATM Networks," *IEEE Communications Magazine*, Vol. 35, No. 11, Nov. 1997.

[8] IEEE. 802.11, IEEE Standard for Wireless LAN Medium Access Control (MAC) and Physical Layer (PHY) specifications, Nov. 1997.

[9] FCC, "Amendment of the Commission's Rules to Provide for Operation of Unlicensed NII Devices in the 5-GHz Frequency Range," Memorandum Opinion and Order, ET Docket No. 96–102, June 24, 1998.

[10] ETSI, "Radio Equipment and Systems, HIgh PErformance Radio Local Area Network (HIPERLAN) Type 1," European Telecommunication Standard, ETS 300–652, Oct. 1996.

[11] Crow, B. P., I. Widjada, J. G. Kim, and P. T. Sakai, "IEEE 802.11 Wireless Local Area Networks," *IEEE Communications Magazine*, pp. 116–126, Sept. 1997.

[12] Takanashi, H., and R. van Nee, "Merged Physical Layer Specification for the 5-GHz Band," IEEE P802.11-98/72-r1, Mar. 1998.

[13] IEEE, "Supplement to Standard for Telecommunications and Information Exchange Between Systems—LAN/MAN Specific Requirements—Part 11: Wireless MAC and PHY Specifications: High Speed Physical Layer in the 5-GHz Band," P802.11a/D7.0, July 1999.

[14] ETSI, "Broadband Radio Access Networks (BRAN); HIPERLAN Type 2 Technical Specification Part 1—Physical Layer," DTS/BRAN030003-1, Oct. 1999.

[15] Nee, R. van, "OFDM for High Speed Wireless Networks," IEEE P 802.11-97/123, Nov. 1997.